5-1-1976

s-Process Studies: Branching and the Time Scale

Richard A. Ward
Rice University

Michael J. Newman
Rice University

Donald D. Clayton
Clemson University, claydonald@gmail.com

THE ASTROPHYSICAL JOURNAL SUPPLEMENT SERIES, 31:33–59, 1976 May

s-PROCESS STUDIES: BRANCHING AND THE TIME SCALE

RICHARD A. WARD, MICHAEL J. NEWMAN, AND DONALD D. CLAYTON
Department of Space Physics and Astronomy, Rice University
Received 1975 June 30

ABSTRACT

The theory of *s*-process heavy-element formation is reformulated to allow for competition between beta decay and neutron capture at various nuclei along the path. Solutions to the resulting branching network equations are presented (under the assumption of constant temperature and neutron flux) that do not require steady flow for the neutron current. Using the exponential exposure distribution $\rho(\tau) = G \exp(-\tau/\tau_0)$ and recently calculated temperature-dependent beta-decay rates, comparison of several key branches yields the following *average* conditions for the solar-system *s*-process environment: $T \approx 3.1 \times 10^8$ K, $n_n \approx 1.6 \times 10^7$ neutrons cm^{-3}. For $\tau_0 = 0.25\, n$ mb^{-1} we find that about 4.8 neutron captures per exposed iron seed are required over a time of the order of a few thousand years for synthesis of the bulk of the solar-system *s*-process material, with an average neutron capture time ~ 10 years (for $\sigma \sim 500$ mb).

Subject headings: abundances — nucleosynthesis — stars: interiors

That man's the true Conservative who lops the mouldered Branch away. [ALFRED, LORD TENNYSON]

I. INTRODUCTION

This paper has two basic purposes. First we present a mathematical formulation of the *s*-process when competition between neutron capture and beta decay is relevant. The original formulation (Burbidge *et al.* 1957; Clayton *et al.* 1961 hereafter called CFHZ), defined a "standard" *s*-process path by assuming that beta decays of radioactive nuclei always occurred before neutron capture, except for a few very long-lived isotopes which were assumed to capture a neutron instead. Although the possibility of branching has been recognized, the mathematics has in the past been developed for either of the resulting unique chains rather than for the actual competition. This point is nontrivial, for although the *s*-process is linear with respect to abundances so that solutions for differing seed nuclei can be summed, it does not admit linear superpositions of unique but differing paths at branch points. Therefore, a mathematics of branching chains is needed. This paper provides it.

Second, we use the mathematics and nuclear data to evaluate a mean neutron density and temperature for the solar-system *s*-process material. To do so we have made calculations of the weak-decay rates as a function of temperature. The self-consistent solution is taken as the best indication of the mean rate of the *s*-process during its operation, and therefore of its astronomical time scale as well. The entire analysis is in the same spirit as the original estimates (Burbidge *et al.* 1957) of the time scale of the *s*-process, but it is physically and quantitatively more precise. Nonetheless, we will conclude, as did they, that the *s*-process occurred near $T = 3 \times 10^8$ K, which places it in helium burning. The time required for neutron capture by a typical nucleus on the path is of the order of 10 years. Competition between beta decay and neutron capture is thus significant for many of the longer lived beta-unstable nuclei.

II. THE MATHEMATICAL PROBLEM

Each nucleus in the chain is created and destroyed by neutron captures and/or by weak decays. In the case where the decays are either too fast or too slow for competition they can be eliminated from the chain or ignored, respectively. The resulting set of equations for the uniquely defined chain is then the one solved by CFHZ (see also Clayton 1968):

$$\frac{dN_A}{dt} = \langle \sigma v \rangle_{A-1} n_n(t) N_{A-1} - \langle \sigma v \rangle_A n_n(t) N_A \,, \tag{1}$$

where $N_A(t)$ is the abundance of the unique isobar of atomic weight A on the *s*-process path. The time dependence enters explicitly through the free-neutron density $n_n(t)$ and through the temperature dependence of $\langle \sigma v \rangle$.

Rather than write a general equation for the case where beta decays occur at rates competitive with neutron capture, it seems to us clearer to consider a specific example having all relevant features. Consider for this purpose the Kr, Rb, Sr portion of the nuclear chart, as shown in Figure 1. Assume now that the *s*-process chain flows

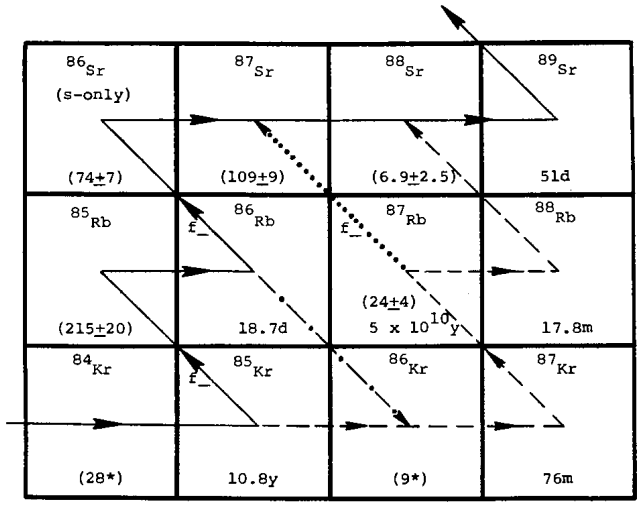

FIG. 1.—The branched *s*-process path through the isotopes of Kr, Rb, and Sr. The arrows indicate the various possible flows leading from ^{85}Kr to ^{88}Sr. Nuclides are labeled with laboratory half-lives and/or neutron-capture cross sections (in mb). An asterisk indicates semiempirical estimates made by Allen *et al.* (1971).

through stable ^{84}Kr and branches due to competition between neutron capture and beta decay at long-lived ^{85}Kr. The equations for the isotopes of Kr, Rb, and Sr involved in the branch are then

$$\begin{aligned}
\frac{dN(^{85}\mathrm{Kr})}{dt} &= \lambda_n(^{84}\mathrm{Kr})N(^{84}\mathrm{Kr}) - [\lambda_-(^{85}\mathrm{Kr}) + \lambda_n(^{85}\mathrm{Kr})]N(^{85}\mathrm{Kr})\,,\\
\frac{dN(^{85}\mathrm{Rb})}{dt} &= \lambda_-(^{85}\mathrm{Kr})N(^{85}\mathrm{Kr}) - \lambda_n(^{85}\mathrm{Rb})N(^{85}\mathrm{Rb})\,,\\
\frac{dN(^{86}\mathrm{Kr})}{dt} &= \lambda_n(^{85}\mathrm{Kr})N(^{85}\mathrm{Kr}) + [\lambda_{ec}(^{86}\mathrm{Rb}) + \lambda_+(^{86}\mathrm{Rb})]N(^{86}\mathrm{Rb}) - \lambda_n(^{86}\mathrm{Kr})N(^{86}\mathrm{Kr})\,,\\
\frac{dN(^{86}\mathrm{Rb})}{dt} &= \lambda_n(^{85}\mathrm{Rb})N(^{85}\mathrm{Rb}) - [\lambda_-(^{86}\mathrm{Rb}) + \lambda_{ec}(^{86}\mathrm{Rb}) + \lambda_+(^{86}\mathrm{Rb})]N(^{86}\mathrm{Rb})\,,\\
\frac{dN(^{86}\mathrm{Sr})}{dt} &= \lambda_-(^{86}\mathrm{Rb})N(^{86}\mathrm{Rb}) - \lambda_n(^{86}\mathrm{Sr})N(^{86}\mathrm{Sr})\,,\\
\frac{dN(^{87}\mathrm{Rb})}{dt} &= \lambda_n(^{86}\mathrm{Kr})N(^{86}\mathrm{Kr}) - [\lambda_n(^{87}\mathrm{Rb}) + \lambda_-(^{87}\mathrm{Rb})]N(^{87}\mathrm{Rb})\,,\\
\frac{dN(^{87}\mathrm{Sr})}{dt} &= \lambda_n(^{86}\mathrm{Sr})N(^{86}\mathrm{Sr}) + \lambda_-(^{87}\mathrm{Rb})N(^{87}\mathrm{Rb}) - \lambda_n(^{87}\mathrm{Sr})N(^{87}\mathrm{Sr})\,,\\
\frac{dN(^{88}\mathrm{Sr})}{dt} &= \lambda_n(^{87}\mathrm{Sr})N(^{87}\mathrm{Sr}) + \lambda_n(^{87}\mathrm{Rb})N(^{87}\mathrm{Rb}) - \lambda_n(^{88}\mathrm{Sr})N(^{88}\mathrm{Sr})\,,
\end{aligned} \tag{2}$$

where $\lambda_n = n_n\langle\sigma v\rangle$ and λ_- is the negatron-decay rate. The electron-capture and positron-emission rates λ_{ec} and λ_+ have been included to illustrate the effect of multiple branching within the main branch itself, although in fact $\lambda_-(^{86}\mathrm{Rb}) \gg \lambda_{ec}(^{86}\mathrm{Rb})$ or $\lambda_+(^{86}\mathrm{Rb})$.

In solving any *s*-process problem, one must decide clearly which assumptions to make. In this case, we are specifically interested in capture and decay competition at ^{85}Kr, whose half-life remains near the laboratory value of 10.8 years to fairly high temperature. In that circumstance we can take ^{86}Rb to have a quasi-static abundance due to its short (18.7 in the laboratory) half-life; therefore,

$$0 = \lambda_n(^{85}\mathrm{Rb})N(^{85}\mathrm{Rb}) - [\lambda_-(^{86}\mathrm{Rb}) + \lambda_{ec}(^{86}\mathrm{Rb}) + \lambda_+(^{86}\mathrm{Rb})]N(^{86}\mathrm{Rb})\,. \tag{3}$$

The differential equations are still hopelessly complicated as long as n_n and T independently depend explicitly and arbitrarily on the time. In such a case there seems no alternative to numerical integration of the equations for each astrophysical problem.

One idealization of clear physical interest, however, is that of a constant-temperature *s*-process. Generally speaking, a given neutron source turns itself on at some temperature and exhausts itself at nearly the same tem-

perature. Even if the temperature is not constant, moreover, the solution at constant temperature is an obvious first approximation to a more general problem. A bonus of this assumption is that the weak rates are also constant (at values determined by T). For the unique chain, where equation (1) is applicable, CFHZ showed that the change of variable from time t to irradiation (or exposure),

$$\tau \equiv \int_0^t n_n(t')v_T dt' , \tag{4}$$

conveniently reduced that equation to

$$\frac{dN_A}{d\tau} = \sigma_{A-1}N_{A-1} - \sigma_A N_A , \tag{5}$$

without any assumption about $n_n(t)$. The convenient solutions and their approximate forms have been discussed by CFHZ, Clayton and Newman (1974), and Clayton and Ward (1974). This simplification is unfortunately not possible in equation (2), because the neutron-capture rates depend explicitly upon $n_n(t)$ whereas the weak-decay rates do not. Therefore time enters in an essential way as an independent variable. For general forms for $n_n(t)$, moreover, the equations can be solved only by numerical integration. A simplification occurs when $n_n(t)$ is also constant. The set of linear first-order differential equations (2) will then have constant coefficients and can be solved explicitly. To examine this problem we use again the variable τ, which in the special case of constant n_n will be linearly proportional to the time.

Because solutions for differing seed nuclei can be superposed, we consider the single most important seed, ^{56}Fe, and use the definition of CFHZ: $\psi(A) = \sigma_A N(A)/N_0(^{56}\mathrm{Fe})$, where $N_0(^{56}\mathrm{Fe})$ is the initial number of ^{56}Fe seed nuclei. Then we can conveniently rewrite equation (2) in matrix form:

$$\frac{d}{d\tau}\mathbf{\Psi} = \boldsymbol{M}\mathbf{\Psi} + \sigma(^{85}\mathrm{Kr})\psi(^{84}\mathrm{Kr})\boldsymbol{e}_1 , \tag{6}$$

where the vectors $\mathbf{\Psi}$ and $\boldsymbol{e}_1$ are defined as

$$\mathbf{\Psi} \equiv \begin{bmatrix} \psi(^{85}\mathrm{Kr}) \\ \psi(^{85}\mathrm{Rb}) \\ \psi(^{86}\mathrm{Kr}) \\ \psi(^{86}\mathrm{Sr}) \\ \psi(^{87}\mathrm{Rb}) \\ \psi(^{87}\mathrm{Sr}) \\ \psi(^{88}\mathrm{Sr}) \end{bmatrix} , \qquad \boldsymbol{e}_1 \equiv \begin{bmatrix} 1 \\ 0 \\ 0 \\ 0 \\ 0 \\ 0 \\ 0 \end{bmatrix} , \tag{7}$$

and the matrix $\boldsymbol{M}$ is as shown in equation (8):

$$\boldsymbol{M} \equiv \begin{bmatrix} \frac{-\sigma(^{85}\mathrm{Kr})}{1-f_-(^{85}\mathrm{Kr})} & 0 & 0 & 0 & 0 & 0 & 0 \\ \frac{f_-(^{85}\mathrm{Kr})\sigma(^{85}\mathrm{Rb})}{1-f_-(^{85}\mathrm{Kr})} & -\sigma(^{85}\mathrm{Rb}) & 0 & 0 & 0 & 0 & 0 \\ \sigma(^{86}\mathrm{Kr}) & [1-f_-(^{86}\mathrm{Rb})]\sigma(^{86}\mathrm{Kr}) & -\sigma(^{86}\mathrm{Kr}) & 0 & 0 & 0 & 0 \\ 0 & f_-(^{86}\mathrm{Rb})\sigma(^{86}\mathrm{Sr}) & 0 & -\sigma(^{86}\mathrm{Sr}) & 0 & 0 & 0 \\ 0 & 0 & \sigma(^{87}\mathrm{Rb}) & 0 & \frac{-\sigma(^{87}\mathrm{Rb})}{1-f_-(^{87}\mathrm{Rb})} & 0 & 0 \\ 0 & 0 & 0 & \sigma(^{87}\mathrm{Sr}) & \frac{f_-(^{87}\mathrm{Rb})\sigma(^{87}\mathrm{Sr})}{1-f_-(^{87}\mathrm{Rb})} & -\sigma(^{87}\mathrm{Sr}) & 0 \\ 0 & 0 & 0 & 0 & \sigma(^{88}\mathrm{Sr}) & \sigma(^{88}\mathrm{Sr}) & -\sigma(^{88}\mathrm{Sr}) \end{bmatrix} . \tag{8}$$

In writing this matrix the symbol f_- has been used for each nucleus as the beta-decay branching ratio $f_- \equiv \lambda_-(\lambda_n + \lambda_- + \lambda_{ec} + \lambda_+)^{-1}$ for that nucleus. It will be a convenient symbol throughout this work. The value of f_- depends explicitly on n_n, depends upon T for those weak rates that depend upon T, and depends on the electron

density n_e whenever electron capture is important or when the exclusion principle is influencing λ_-. The parameters f_- thus depend upon the time through the time dependence of each of these physical quantities; therefore, the elements of the matrix $\boldsymbol{M}$ depend in general upon τ. The special problem we will consider is that of constant n_n and constant thermal environment, so that each f_- is constant. The matrix $\boldsymbol{M}$ is then also constant. Physically this means that we assume that the neutron flux rises quickly from zero as the neutron-liberating reactions begin, remains reasonably constant, and finally falls to zero in a time much shorter than the duration of the irradiation. To make the usual comparisons with nuclear abundances outside of stars, in fact, we assume that $n_n(t)$ falls to zero so quickly that the nuclear abundances are frozen against further modification by neutron capture (although the weak decays of course continue until all active species have decayed to their stable isobars). This last assumption is not necessarily the way in which the *s*-process has actually frozen, but it is the simplest assumption and can in any case be modified by specific terminal alterations whenever one thinks he has a model for the freezing of *s*-process nuclei.

Although the model problem we will solve is an idealization of the physical *s*-process, the assumption of constant f_- is a useful generalization of the traditional simplification that $f_- = 1$ for all decaying nuclei. Since the several f_- depend upon T, moreover, we can seek that value of T that best reproduces observed abundances. We therefore return to equation (6), initially following the work of Clayton and Rassbach (1967), and consider the matrix $\boldsymbol{M}$ to be constant.

Before proceeding it is worthwhile to note the "lower triangular" form of $\boldsymbol{M}$ in equation (8), which is typical of *s*-process branching in that the only contribution to the abundance of a nucleus of atomic weight A comes from nuclei having $A' \leq A$. That is, there is generally no cycling due to alpha decay except in special cases studied by Clayton and Rassbach (1967) and Perrone and Clayton (1971). Because $\boldsymbol{M}$ is of lower triangular form, its eigenvalues are merely its diagonal elements (which are always negative). As long as these eigenvalues (cross sections or combinations of cross sections and branching ratios) are distinct, $\boldsymbol{M}$ can be decomposed as

$$\boldsymbol{M} = \boldsymbol{ABA}^{-1} \tag{9}$$

where $\boldsymbol{B}$ is the diagonal matrix of eigenvalues, $\boldsymbol{B} = \mathrm{diag}(\beta_1, \ldots, \beta_7)$, and A is the matrix of column eigenvectors. The mathematical problem of degenerate eigenvalues can always be circumvented by merely adjusting the values of the cross sections in some small way consistent with their experimental uncertainties. In the applications to be presented later, this problem has proven to have negligible effect on the computed results. Multiplying equation (6) on the left by $\boldsymbol{A}^{-1}$ yields, with equation (9),

$$\frac{d}{d\tau}(\boldsymbol{A}^{-1}\boldsymbol{\Psi}) = \boldsymbol{B}(\boldsymbol{A}^{-1}\boldsymbol{\Psi}) + \sigma(^{85}\mathrm{Kr})\psi(^{84}\mathrm{Kr})(\boldsymbol{A}^{-1}\boldsymbol{e}_1)\,. \tag{10}$$

The solution to the eigenvalue equation (9) will admit in this case 7 undetermined constants corresponding to the normalization of each eigenvector. These may be conveniently fixed by requiring

$$(\boldsymbol{A}^{-1}\boldsymbol{e}_1) = \begin{bmatrix} 1 \\ \vdots \\ 1 \end{bmatrix}. \tag{11}$$

Using equation (11) in equation (10) and recalling that $\boldsymbol{B}$ is diagonal yields the set of *uncoupled* differential equations

$$\frac{d}{d\tau}(\boldsymbol{A}^{-1}\boldsymbol{\Psi})_i = \beta_i(\boldsymbol{A}^{-1}\boldsymbol{\Psi})_i + \sigma(^{85}\mathrm{Kr})\psi(^{84}\mathrm{Kr})\,, \tag{12}$$

which are easily integrated with the boundary condition $\boldsymbol{\Psi}(0) = \boldsymbol{0}$ to give

$$(\boldsymbol{A}^{-1}\boldsymbol{\Psi})_i = \exp(\beta_i\tau)\int_0^\tau \exp(-\beta_i\tau')\,\sigma(^{85}\mathrm{Kr})\psi(^{84}\mathrm{Kr})d\tau'\,. \tag{13}$$

Regarding this set of functions as a column vector and left-multiplying by $\boldsymbol{A}$ gives

$$\boldsymbol{\Psi} = \boldsymbol{A}\begin{bmatrix} (\boldsymbol{A}^{-1}\boldsymbol{\Psi})_1 \\ \vdots \\ (\boldsymbol{A}^{-1}\boldsymbol{\Psi})_7 \end{bmatrix}, \tag{14}$$

or in component form,

$$\psi_i(\tau) = \sigma(^{85}\mathrm{Kr})\sum_{j=1}^{7} A_{ij}\exp(\beta_j\tau)\int_0^\tau \exp(-\beta_j\tau')\psi(^{84}\mathrm{Kr}, \tau')d\tau'\,, \tag{15}$$

which is the desired result. It expresses $\psi_i(\tau)$ for the nuclei within the branch in terms of ψ for the nucleus just preceding the branch (in this example ^{84}Kr) and in terms of the cross sections and branching ratios within the branch. To use it one needs only the normalized matrix of column eigenvectors A, which is easily obtained in standard fashion.

To evaluate ψ_i one needs the functional form of the source term $\psi(^{84}\mathrm{Kr})$. If the branch is not too far removed from the iron seed (where "far" is determined by the numerical difficulty involved), one can use the exact functional form of the source term; alternatively, and more commonly, one must use a manageable approximate form for the source term. Another problem of interest occurs whenever one is interested in a distribution of irradiations τ. We analyze these alternatives in what follows.

a) Exact Source Term

CFHZ showed that if the path is unique up to ^{84}Kr, then $\psi(^{84}\mathrm{Kr})$ can be written

$$\psi(^{84}\mathrm{Kr};\ \mathrm{Unique}) = \sum_{i=56}^{84} C_{84,i} \exp(-\sigma_i \tau)\,, \tag{16}$$

where the $C_{84,i}$ are a set of (in this case) 29 constants. In § III, equation (43), we will show that if there are p distinct branches of the type we have discussed between $A = 56$ and $A = 84$, which is itself unique, the exact form is then a more complicated sum of exponentials:

$$\psi(^{84}\mathrm{Kr};\ p\ \mathrm{branches}) = \sum_{k\ldots q} a_k^{(1)} \ldots a_q^{(p)} \sum_{r=56}^{84} C_{84,r}^{k\ldots q} \exp(-\eta_r \tau)\,, \tag{17}$$

where the notation will be explained more fully in § III. Equation (17) reduces to equation (16) if there are no branches before ^{84}Kr. In either case, the exact source term can be integrated explicitly in equation (15) to give for each of the seven nuclei designated i in the branch following ^{84}Kr

$$\psi_i(\tau) = \sigma(^{85}\mathrm{Kr}) \sum_{k\ldots q,j} a_k^{(1)} \ldots a_q^{(p)} A_{ij} \sum_{r=56}^{84} C_{84,r}^{k\ldots q} \left(\frac{\exp(\beta_j \tau) - \exp(-\eta_r \tau)}{\beta_j + \eta_r} \right)\,. \tag{18}$$

This solution, though exact, suffers from the same numerical difficulty that CFHZ found surrounding even equation (16). It is therefore more useful to consider the CFHZ approximation to the source term, especially since it has been shown (Clayton and Newman 1974; Clayton and Ward 1974) that this approximation well represents the exact solution.

b) Approximate CFHZ Source Term

Following CFHZ, we write as an approximation

$$\psi(^{84}\mathrm{Kr};\ \mathrm{CFHZ}) = \lambda \frac{(\lambda\tau)^{m-1}}{\Gamma(m)} e^{-\lambda\tau}\,, \tag{19}$$

where the parameters λ and m depend on all the cross sections between the seed nucleus and ^{84}Kr and, as we will show in § III, upon intervening branches, if any, between the seed nucleus and ^{84}Kr. With this form equation (15) can be integrated to give

$$\psi_i(\tau) = \psi(^{84}\mathrm{Kr};\ \mathrm{CFHZ}) \frac{\sigma(^{85}\mathrm{Kr})\tau}{m} \sum_{j=1}^{7} A_{ij} M[1,\ 1 + m,\ (\lambda + \beta_j)\tau]\,, \tag{20}$$

where $M(a, b, x)$ is the confluent hypergeometric function

$$M(a, b, x) = \sum_{l=0}^{\infty} \frac{(a)_l x^l}{l!(b)_l}\,, \tag{21}$$

and the Pochhammer symbol $(a)_l = a(a + 1)\ldots(a + l - 1)$ with $(a)_0 \equiv 1$. This result goes properly to zero as $\tau \to 0$ and as $\tau \to \infty$, having in fact considerable similarity to the more common CFHZ form (19).

c) Superposition of Irradiations

Since CFHZ it has been known that the distribution of *s*-process abundances observed in the solar system is a superposition of differing numbers of seed nuclei $\rho(\tau)$ exposed to irradiation τ per interval $d\tau$:

$$(\sigma N)_A = \int_0^{\infty} \rho(\tau)\psi(A)d\tau\,. \tag{22}$$

CFHZ presented evidence that $\rho(\tau)$ is a decreasing function of τ. Seeger, Fowler, and Clayton (1965) suggested that it might be approximated well by an exponential distribution

$$\rho(\tau) = G \exp(-\tau/\tau_0), \tag{23}$$

and presented the resulting solution $(\sigma N)_A$ based on the CFHZ approximation for a unique path. Clayton and Ward (1974) later showed that those superpositions based on the CFHZ approximation have adequate accuracy for most astrophysical problems.

For our present study of abundances resulting from branches, we return to the exact relationship (15) within the ^{85}Kr branch in conjunction with an assumed distribution (23):

$$(\sigma N)_i = G\sigma(^{85}\mathrm{Kr}) \sum_{j=1}^{7} A_{ij} \int_0^\infty d\tau \{\exp[-(\tau/\tau_0) + \beta_j\tau]) \int_0^\tau \exp(-\beta_j\tau')\psi(^{84}\mathrm{Kr}, \tau')d\tau'\}. \tag{24}$$

Upon performing the integration over τ, we find that

$$(\sigma N)_i = (\sigma N)_{84} \sum_{j=1}^{7} \frac{A_{ij}\sigma(^{85}\mathrm{Kr})}{(1/\tau_0) - \beta_j}, \tag{25}$$

where we have used the definition for unique ^{84}Kr,

$$(\sigma N)_{84} = \int_0^\infty G \exp(-\tau'/\tau_0)\psi(^{84}\mathrm{Kr})d\tau'. \tag{26}$$

This result is particularly useful in that Seeger, Fowler, and Clayton (1965), Ulrich (1973), and Clayton and Ward (1974) have each confirmed the plausibility and good abundance fit of the exponential distribution. We will return to it in the next section. It is also *exact*, in the sense that no mathematical approximation has been made, that no specific form for $\psi(^{84}\mathrm{Kr})$ was assumed, and therefore that no specific assumption concerning the identity and abundances of seed nuclei $A \leq 84$ was made. This independence from the seed distribution has previously been demonstrated for the exponential distribution of exposures in the case of a unique chain by Clayton and Ward (1974). It also implies in this case that if i and k designate any two nuclei within the branch, then

$$\frac{(\sigma N)_i}{(\sigma N)_k} = \sum_{j=1}^{7} A_{ij}(1 - \tau_0\beta_j)^{-1} \Big/ \left[\sum_{j=1}^{7} A_{kj}(1 - \tau_0\beta_j)^{-1}\right]. \tag{27}$$

That this ratio does not depend upon the form of $\psi(\tau)$ for the source term is a result exactly true only for an exponential $\rho(\tau)$. We have also solved equation (15) for the power-law distribution $\rho(\tau) = (\tau/\tau_0)^{-n}$, which was studied by Seeger, Fowler, and Clayton (1965) and Seeger and Fowler (1966) for the unique chain. In this case, the exact source term yields a sum of gamma functions. If we take the simpler approximate source term (19), we find, for nuclei with cross sections sufficiently small that $\lambda > |\lambda + \beta_j|$, the following result:

$$(\sigma N)_i = \frac{(\lambda\tau_0)^n\sigma(^{85}\mathrm{Kr})\Gamma(1 + m - n)}{\Gamma(1 + m)} \sum_{j=1}^{7} \left(\frac{A_{ij}}{\lambda}\right) F\left(1, 1 + m - n; 1 + m; 1 + \frac{\beta_j}{\lambda}\right), \tag{28a}$$

and for the large cross sections, where $-\beta_j > |\lambda + \beta_j|$,

$$(\sigma N)_i = \frac{(\lambda\tau_0)^n\sigma(^{85}\mathrm{Kr})\Gamma(1 + m - n)}{\Gamma(1 + m)} \sum_{j=1}^{7} \left(\frac{A_{ij}}{-\beta_j}\right) F\left(1, n; 1 + m; 1 + \frac{\lambda}{\beta_j}\right), \tag{28b}$$

where F is Gauss's hypergeometric function

$$F(a, b; c; z) = \sum_{l=0}^{\infty} \frac{(a)_l(b)_l z^l}{l!(c)_l},$$

and the Pochhammer symbol $(a)_l$ was defined in equation (21). Equations (28a) and (28b) give the same result for those intermediate values of β_j for which both inequalities are satisfied. With this superposition of exposures the ratio $(\sigma N)_i/(\sigma N)_k$ still depends on the form of $\psi(^{84}\mathrm{Kr})$, as shown explicitly by the dependence on both m and λ. We have used this result successfully in some of our studies but have a certain prejudice against it for physical reasons, namely that the power-law distribution must be cut off in unknown ways at small τ to avoid the divergence of total seed, and perhaps at large τ to avoid overabundances of Pb isotopes. If one wishes a distribution that falls more rapidly at small τ and more slowly at large τ than a single exponential, it seems preferable to go to a sum of exponentials, namely,

$$\rho(\tau) = G_1 \exp(-\tau/\tau_{01}) + G_2 \exp(-\tau/\tau_{02}), \tag{29}$$

where $\tau_{01} < \tau_{02}$ and $G_1 > G_2$. Due to the linearity of the equations, each $(\sigma N)_i$ is then the simple sum of two parts that can be calculated exactly and without cutoffs. With this in mind, we will prefer to restrict our displayed equations to the single exponential.

d) Limit of Steady Flow

The usual *s*-process time-scale arguments hinge on the assumption of steady flow ($d\mathbf{\Psi}/d\tau = \mathbf{0}$) of the neutron current through the branching network. The above results are not so restricted and can be used in rapidly falling portions of the σN curve. Nonetheless it is useful to see how this treatment reduces to that of steady flow. In the regions *between* closed-shell nuclei, $-\beta_j$ is typically a few hundred millibarns, which is much greater than $1/\tau_0$ or λ. In that case equations (20) (for $-\beta_j\tau \gg 1$), (25), and (28b) all yield the same asymptotic equilibrium ratio:

$$\frac{(\sigma N)_i}{(\sigma N)_k} \approx \frac{\Sigma_j A_{ij}/\beta_j}{\Sigma_j A_{kj}/\beta_j} . \tag{30}$$

Examination of the relevant matrices shows that the sums on the right-hand side are equal to

$$\begin{bmatrix} \Sigma_j A_{1j}/\beta_j \\ \vdots \\ \Sigma_j A_{7j}/\beta_j \end{bmatrix} = \boldsymbol{M}^{-1}\boldsymbol{e}_1 . \tag{31}$$

On the other hand, the product $\boldsymbol{M}^{-1}\boldsymbol{e}_1$ can be obtained from equation (6) by left-multiplying by $\boldsymbol{M}^{-1}$ and integrating over τ:

$$-\boldsymbol{M}^{-1}\boldsymbol{e}_1 = \frac{\int_0^\infty \mathbf{\Psi}(\tau)d\tau - \boldsymbol{M}^{-1}[\mathbf{\Psi}(\infty) - \mathbf{\Psi}(0)]}{\sigma(^{85}\mathrm{Kr})\int_0^\infty \psi(^{84}\mathrm{Kr})d\tau} \tag{32}$$

The boundary conditions are $\mathbf{\Psi}(0) = \mathbf{\Psi}(\infty) = \mathbf{0}$; furthermore, since ^{84}Kr is a unique (i.e., nonbranched) isobar, all of the seed nuclei must pass through it, giving $\int_0^\infty \psi(^{84}\mathrm{Kr})d\tau = 1$. Thus

$$-\boldsymbol{M}^{-1}\boldsymbol{e}_1 = \frac{1}{\sigma(^{85}\mathrm{Kr})}\int_0^\infty \mathbf{\Psi}(\tau)d\tau . \tag{33}$$

Since $\int_0^\infty \psi_i(\tau)d\tau = f_i$ is the fraction of the flow passing through species i, equations (33) and (30) show

$$\frac{(\sigma N)_i}{(\sigma N)_k} \approx \frac{f_i}{f_k} , \tag{34}$$

which is the expression used in previous branching calculations (e.g., Peterson and Tripp 1973). Our own analysis of several branches using our non–steady-flow results will be described in § IV.

e) $\psi_i(\tau)$ for ^{85}Kr Example

Although the solar-system abundances are a superposition of exposures, the observation of freshly produced heavy elements on the surfaces of individual stars could require knowledge of $\mathbf{\Psi}(\tau)$ directly. To illustrate these results, Figures 2 and 3 show plots of equation (20) for the various members of the ^{85}Kr branch calculated with typical values of $f_-(^{85}\mathrm{Kr})$ and $f_-(^{87}\mathrm{Rb})$. Because ^{85}Kr has a short (10.8 years in the laboratory) half-life as far as observed abundances are concerned, its $\psi(\tau)$ must be added to that of ^{85}Rb (in Fig. 2), weighted with the factor $\sigma(^{85}\mathrm{Rb})/\sigma(^{85}\mathrm{Kr})$. Figure 3 also shows how poor the steady-flow approximation is in this region, because under it the seven ψ_i would maintain the same ratios to each other at differing values of τ. Figure 4 results from setting the ratio $\psi(^{86}\mathrm{Sr})/\psi(^{88}\mathrm{Sr})$ equal to different multiples of its observed solar value and then finding for each value of $f_-(^{85}\mathrm{Kr})$ the value of τ at which that ratio is achieved. This figure is not so much observationally useful as it is illustrative of the potential sensitivity of the branching interrelationships.

III. COMPLETE *s*-PROCESS WITH BRANCHING

We will now examine the cumulative effect of all of the individual branches on the overall *s*-process σN curve. The previous section gave the results for members within a branch, so we will concentrate here on the *unique* isobars that lie in atomic weight between the various branching networks. To this end we may generalize equation (15) to apply to the ith branch, which begins after unique nucleus b (for *beginning*) and ends with unique nucleus l (for *last*). Writing that result for this last nucleus l and letting parenthetical superscript (i) designate quantities as belonging to the ith branch, we have

$$\psi_l^{(i)}(\tau) = \sigma_{b+1}^{(i)} \sum_j A_{lj}^{(i)} \exp(\beta_j^{(i)}\tau) \int_0^\tau \exp(-\beta_j^{(i)}\tau')\psi_b^{(i)}(\tau')d\tau' , \tag{35}$$

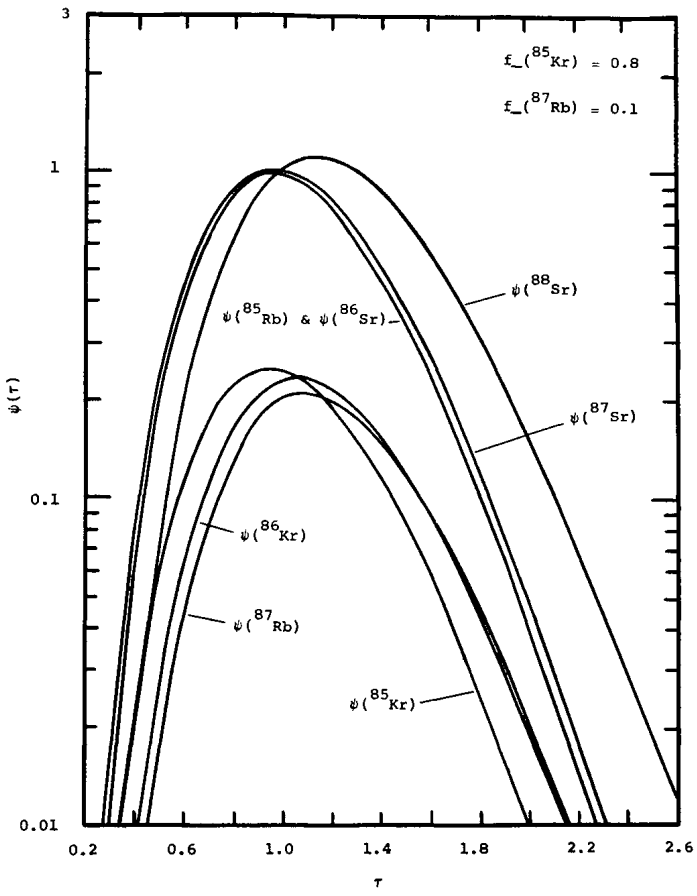

FIG. 2

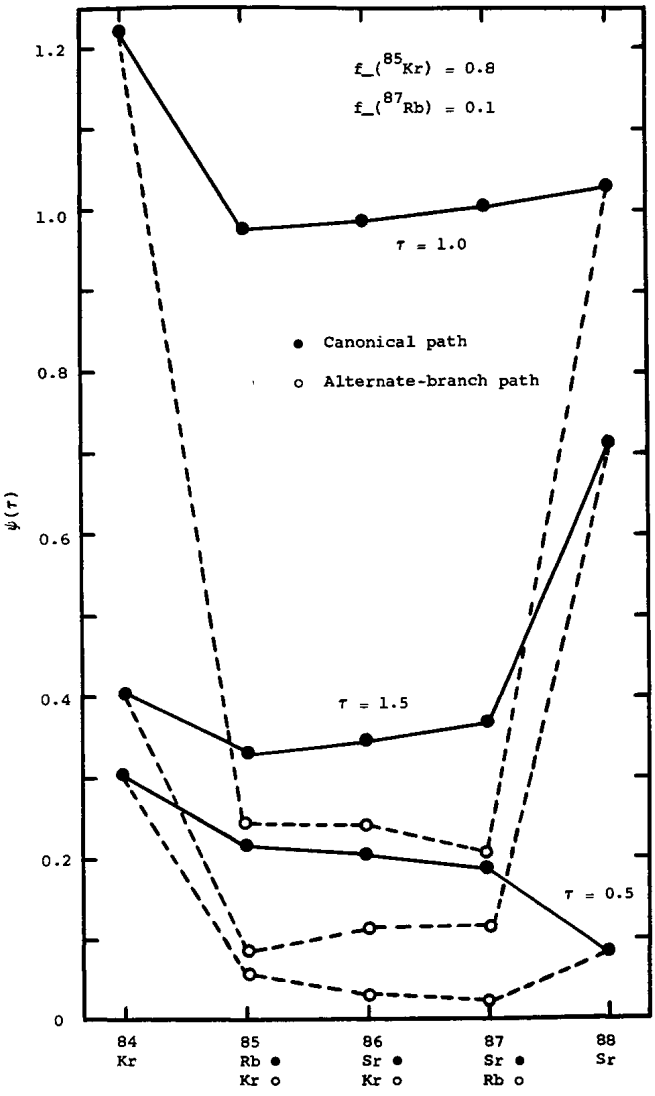

FIG. 3

FIG. 2.—Variation of $\psi(\tau)$ versus τ for the members of the ^{85}Kr branch system for various branching ratios

FIG. 3.—The same data as in Fig. 2 replotted to better illustrate the relative abundance flow through each isotope at typical values of τ.

where $\sigma_{b+1}{}^{(i)}$ is the branch-point cross section immediately following unique beginning nucleus b. Note that b and l, as unique s-process isobars, could also be designated by their atomic weights, which were respectively 84 and 88 in the example ^{85}Kr branch; but the number of intervening species j is necessarily greater than the difference of initial and final unique atomic weights. As a final clarification before continuing, we note a change of indexing from the ^{85}Kr example to subscripts, so that for that branch we now have $\psi(^{84}\mathrm{Kr}) = \psi_b$ and $\psi(^{88}\mathrm{Sr}) = \psi_l$.

For subsequent analysis we will find, as did CFHZ, that the Laplace transforms of the ψ functions will be useful. They are designated by a bar on top; for example,

$$\bar{\psi}_l{}^{(i)}(s) \equiv \int_0^\infty e^{-s\tau}\psi_l{}^{(i)}(\tau)d\tau\,, \tag{36}$$

which for equation (35) gives

$$\bar{\psi}_l{}^{(i)}(s) = \sigma_{b+1}{}^{(i)} \sum_j A_{lj}{}^{(i)} \int_0^\infty d\tau \left[\exp\left(-s\tau + \beta_j{}^{(i)}\tau\right) \int_0^\tau \exp\left(-\beta_j{}^{(i)}\tau'\right)\psi_b{}^{(i)}(\tau')d\tau'\right]. \tag{37}$$

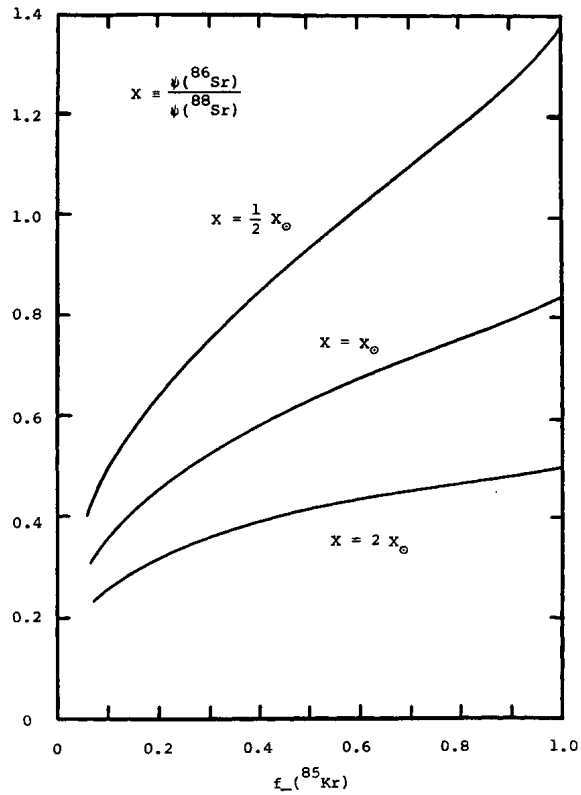

FIG. 4.—Values of τ as a function of $f_{-}(^{85}\mathrm{Kr})$ required to make $\psi(^{86}\mathrm{Sr})/\psi(^{88}\mathrm{Sr})$ equal to different multiples of the observed solar-system value $X_\odot = 1.45$.

Rearranging the limits of the integrals, one finds at once

$$\bar{\psi}_l^{(i)}(s) = \bar{\psi}_b^{(i)}(s) \sum_j \frac{\sigma_{b+1}^{(i)} A_{lj}^{(i)}}{s - \beta_j^{(i)}} \,. \tag{38}$$

This important result, which can also be obtained by solving algebraically the Laplace transform of the set of differential equations, shows that the Laplace transform for the function $\bar{\psi}_l^{(i)}$ at the end of branch i is proportional to the Laplace transform $\bar{\psi}_b^{(i)}$ at the beginning of that branch. The factor relating them is a type of "transfer function" that depends on the detailed properties within the branch itself. For comparison it is worth noting, as is shown below, that if there was in fact no branch between b and l, the transfer function could be written in the form found by CFHZ, which is

$$\prod_j \sigma_j/(s + \sigma_j) \,,$$

a product of the unique s-process nuclei between $b + 1$ and l. In such a case, $\beta_j \to -\sigma_j$, the number of terms j becomes equal to $l - b$, and the A_{lj} are such that the sum coalesces to this simple product.

For any unique s-process isobar $A(> l)$ beyond the ith branch but before the $(i + 1)$th branch, CFHZ showed

$$(s + \sigma_A)\bar{\psi}_A(s) = \sigma_A \bar{\psi}_{A-1}(s) \tag{39}$$

so that in terms of $\bar{\psi}_l^{(i)}$ we have the transfer product mentioned above,

$$\bar{\psi}_A(s) = \frac{\sigma_A \cdots \sigma_{l+1}}{(s + \sigma_A) \cdots (s + \sigma_{l+1})} \bar{\psi}_l^{(i)}(s) \,, \tag{40}$$

which using equation (38) may be related to the beginning of branch i as

$$\bar{\psi}_A(s) = \left(\prod_{l+1}^{A} \frac{\sigma_m}{s + \sigma_m} \right) \sum_j \frac{\sigma_{b+1}^{(i)} A_{lj}^{(i)}}{s - \beta_j^{(i)}} \bar{\psi}_b^{(i)}(s) \,. \tag{41}$$

We may easily generalize this result back to seed ^{56}Fe by including the effect of all antecendent branches, taken to be p in number,

$$\bar{\psi}_A(s) = \left(\prod_{m=56}^{A} \frac{\sigma_m}{s+\sigma_m}\right)\left(\sum_j \frac{a_j^{(1)}}{s-\beta_j^{(1)}}\right)\cdots\left(\sum_{j'} \frac{a_{j'}^{(p)}}{s-\beta_{j'}^{(p)}}\right), \tag{42}$$

where we have introduced the abbreviated notation $a_k^{(i)} \equiv \sigma_{b+1}{}^{(i)} A_{lk}^{(i)}$. The first product includes only the unique s-process isobars, but excluding those designated l at the branch end points, between 56 and A. Inverting the Laplace transform (42) and evaluating the integral by closing the contour with a semicircular path in the left half of the complex plane, we find

$$\psi_A(\tau) = \sum_{j\cdots j'} a_j^{(1)}\cdots a_{j'}^{(p)} \sum_{r=56}^{A} C_{A,r}^{j\cdots j'} \exp(-\eta_r\tau), \tag{43}$$

where

$$C_{A,r}^{j\cdots j'} = \frac{\sigma_A\cdots\sigma_{56}}{(\sigma_A-\eta_r)(-\beta_{j'}^{(p)}-\eta_r)\cdots(-\beta_j^{(1)}-\eta_r)(\sigma_{56}-\eta_r)},$$

with the term $(\eta_r - \eta_r)$ deleted from the denominator of C. The sum over η_r includes each pole of the integrand—the cross sections σ_r at the unique isobars and the eigenvalues $-\beta_r$ of the branching-network matrices. The multiple sums in equation (43) physically represent taking all possible combinations of branched paths leading to the unique isobar A and then superposing them with each path weighted by the probability of its occurrence. Equation (43) applies only to the unique s-process isobars, but it can also be used as the exact source term for obtaining $\psi(\tau)$ for the nuclides within a branch, as was described in equation (18), which was written for the example ^{85}Kr branch but is trivially generalizable to any other branch.

a) CFHZ Approximation

Equations (43) and (18) suffer from a severe difficulty. They contain so many terms for $A > 100$, say, that they are extremely treacherous to evaluate. There is so much approximate cancellation among terms that round-off error is almost unmanageable. To circumvent this trouble CFHZ introduced the approximation to the Laplace transform

$$\bar{\psi}_A(s) \approx \left(1+\frac{s}{\lambda_A}\right)^{-m_A}, \tag{44}$$

which has been shown to lead upon inversion to an excellent approximation to $\psi_A(\tau)$ in the significant domain (Clayton and Newman 1974; Clayton and Ward 1974), namely equation (19). We wish to adopt the same approximation for the unique s-process isobars; however, the intervening branches will alter the prescription for generating the parameters λ_A and m_A. In what follows we derive the appropriate prescription. The approximation sought is

$$\left[\sum_j \frac{a_j^{(1)}}{s-\beta_j^{(1)}}\cdots\sum_{j'}\frac{a_{j'}^{(p)}}{s-\beta_{j'}^{(p)}}\right]\Big/\left[\left(1+\frac{s}{\sigma_A}\right)\cdots\left(1+\frac{s}{\sigma_{56}}\right)\right] \approx \left(1+\frac{s}{\lambda_A}\right)^{-m_A}. \tag{45}$$

Following CFHZ we seek the best approximation for small values of s, corresponding to large values of τ. Both sides go to unity at $s = 0$, the left side doing so by virtue of

$$\sum_j \sigma_{b+1}{}^{(i)} A_{lj}^{(i)}/\beta_j^{(i)} = -1.$$

Since the right-hand side contains only two parameters, the equality can be guaranteed only for the first- and second-order terms in the power series expansions in s. These are, respectively,

first order:

$$\sum_{k=1}^{A}\frac{1}{\sigma_k} + \Lambda_A = \frac{m_A}{\lambda_A}, \tag{46}$$

second order:

$$\sum_{k=1}^{A}\left(\frac{1}{\sigma_k}\right)^2 + \Lambda_A\sum_{k=1}^{A}\frac{1}{\sigma_k} + \chi_A + \Omega_A + \sum_{r<p}^{A}\frac{1}{\sigma_r\sigma_p} = \frac{m_A(m_A+1)}{2\lambda_A{}^2}, \tag{47}$$

where we define the following sums:

$$\Lambda_A^{(p)} \equiv \sum_j a_j^{(1)}(\beta_j^{(1)})^{-2} + \cdots + \sum_{j'} a_{j'}^{(p)}(\beta_{j'}^{(p)})^{-2},$$

$$\chi_A^{(p)} \equiv \sum_j a_j^{(1)}(\beta_j^{(1)})^{-3} + \cdots + \sum_{j'} a_{j'}^{(p)}(\beta_{j'}^{(p)})^{-3},$$

$$\Omega_A^{(p)} \equiv \sum_{i<k}^{p} \left[\sum_j a_j^{(i)}(\beta_j^{(i)})^{-2} \sum_{j'} a_{j'}^{(k)}(\beta_{j'}^{(k)})^{-2}\right].$$

These parameters Λ_A, χ_A, and Ω_A are less complicated than they look. Each sum

$$\sum_j a_j^{(i)}(\beta_j^{(i)})^{-n}$$

need be calculated only once for each branch (once the environment is fixed). Each parameter has the same value for all values of A between two adjacent branches; that is, their values change only when another new branch has been added to the chain. They are, in fact, constants associated with the number of preceding branches p, and are therefore so designated. The sums $\sum (1/\sigma_k)^n$ rather clearly contain only the unique isobars, excluding branch ends, out to atomic weight A.

Solving equations (46) and (47) for λ_A and m_A gives

$$\lambda_A = \frac{\sum (1/\sigma_k) + \Lambda_A}{\sum (1/\sigma_k)^2 + 2\chi_A - \xi_A}, \tag{48}$$

and

$$m_A = \frac{[\sum (1/\sigma_k) + \Lambda_A]^2}{\sum (1/\sigma_k)^2 + 2\chi_A - \xi_A}, \tag{49}$$

where

$$\xi_A = \Lambda_A^2 - 2\Omega_A = \sum_{i=1}^{p}\left[\sum_j a_j^{(i)}(\beta_j^{(i)})^{-2}\right]^2.$$

The values of λ_A and m_A given in equations (48) and (49) may be used in equation (19), in exact analogy to the CFHZ approximation. With no branching at all, these parameters reduce explicitly to the values given by CFHZ.

As a numerical example of the effect of preceding branches on the value of $\psi_A(\tau)$, we consider the changes brought about on $\psi(^{90}\mathrm{Zr})$ by branches at ^{79}Se and ^{85}Kr. The function $\psi_{90}^{\text{Unique}}$ is calculated with equation (19) under the assumptions that ^{79}Se always captures a neutron and that ^{85}Kr always beta decays. The function $\psi_{90}^{\text{Branched}}$ is also calculated with equation (19), but with various assumptions regarding $f_-(^{79}\mathrm{Se})$ and $f_-(^{85}\mathrm{Kr})$ leading to the new values of λ_A and m_A. Figure 5 shows the ratio of the two functions calculated with two different values of $f_-(^{79}\mathrm{Se})$ for each of three different values of $f_-(^{85}\mathrm{Kr})$. Order-of-magnitude differences are evident, as is the fact that the value of $f_-(^{85}\mathrm{Kr})$ has the stronger effect. Physically what happens is that the flow through ^{86}Kr is delayed by the smaller cross sections at ^{86}Kr and ^{87}Rb relative to the flow through ^{86}Sr and ^{87}Sr. Figure 6 shows directly the dependence of the ratio on $f_-(^{85}\mathrm{Kr})$ for selected values of τ. These two figures show that the effect of branching can be large.

b) Superposition of Irradiations

For the σN curve observed in the solar system we must again form a superposition as in equation (22). For the exponential exposure distribution $\rho(\tau) = G \exp(-\tau/\tau_0)$ we note (Clayton and Ward 1974) that the superposition (22) is the same integral as the Laplace transform with s replaced by $1/\tau_0$, and can write down immediately from equation (42)

$$(\sigma N)_A = G \prod_{i=1}^{p}\left[\sum_j \frac{a_j^{(i)}}{(1/\tau_0) - \beta_j^{(i)}}\right] \prod_{m=56}^{A}\left(1 + \frac{1}{\tau_0 \sigma_m}\right)^{-1}, \tag{50}$$

where the product over m includes the unique isobars but excludes the branch end points. This result is very useful considering that the exponential distribution is so physically attractive. It also generalizes easily for $\rho(\tau)$ in the form of equation (29).

We again illustrate this effect by showing in Figure 7 the manner in which $(\sigma N)_{90}$ depends upon $f_-(^{85}\mathrm{Kr})$, for two specific values each of $f_-(^{79}\mathrm{Se})$ and of τ_0. These effects, which are clearly substantial, can again be understood in terms of the relative delay of the flow through the branch having the smaller cross sections.

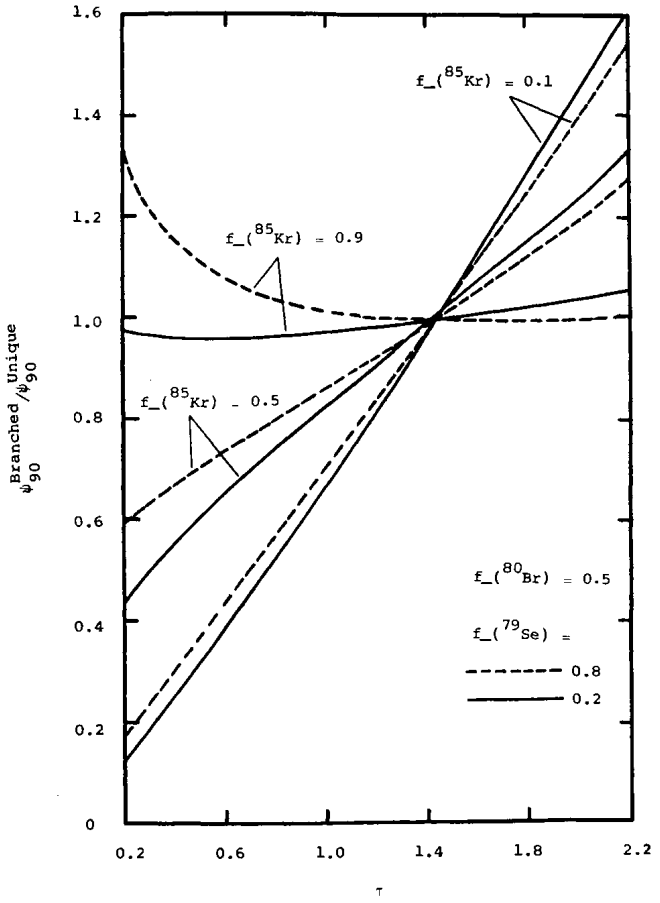

FIG. 5

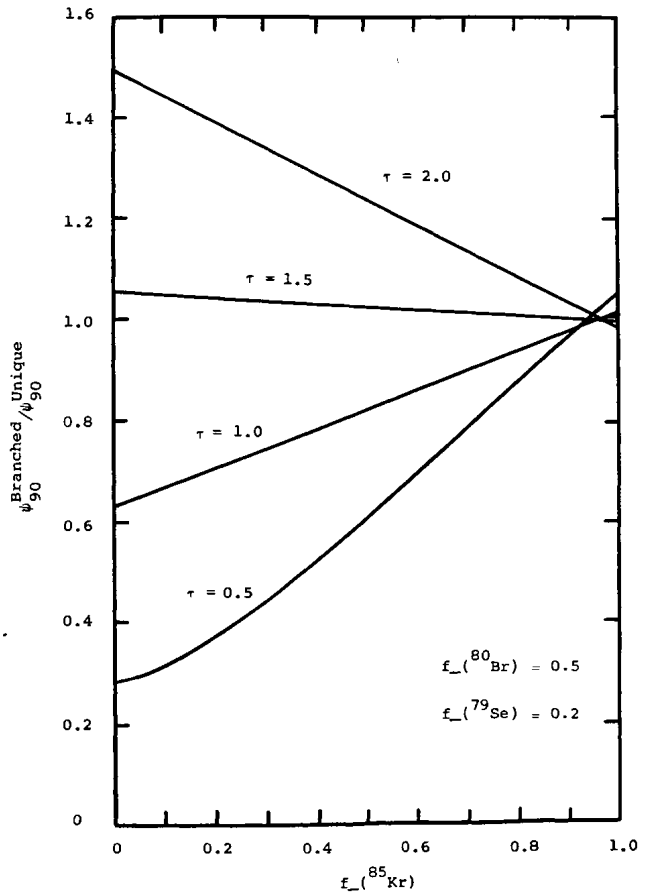

FIG. 6

FIG. 5.—The effect of the *s*-process branches at ^{79}Se and ^{85}Kr on the value of $\psi(^{90}\text{Zr})$ as a function of τ. The value of $\psi(^{90}\text{Zr})$ is expressed as a multiple of the value it would have in the absence of branching.

FIG. 6.—The pronounced effect on ψ_{90} caused by the small cross section at ^{86}Kr as a function of $f_{-}(^{85}\text{Kr})$ for typical values of the neutron exposure.

So significant is this relative-delay effect that we choose to illustrate it quantitatively with the example of two alternate extremes of the very simple branch shown in the inset of Figure 8. The beta decays are very fast, but the first one is either a β^- emission or a β^+ emission, so that the capture path passes through either σ_1 or σ_2, respectively. For any unique nucleus beyond this branch, the ratio of the σN value obtained by passing solely through σ_2 to that obtained by passing solely through σ_1 is, from equation (50), equal to

$$\mathscr{R} = \frac{\sigma_2(1 + \tau_0\sigma_1)}{\sigma_1(1 + \tau_0\sigma_2)} . \tag{51}$$

In Figure 8 we plot $\mathscr{R}$ for $\sigma_1 = 100$ mb (a typical capture cross section) as a function of σ_2 for several values of the parameter τ_0 characterizing the exponential distribution of exposures. Because the ratio is independent of A, all subsequent nuclei suffer the same shift in their σN value. Since the solar-system abundances are characterized by values near $\tau_0 = 0.2$ to 0.3, the effect is significant.

Equation (50) has another very important property, one that was first demonstrated for the unique chain by Clayton and Ward (1974), namely, the shape of the curve beyond the seed nuclei is independent of the identity of the seed nuclei. That the same is true within a branch is clear from equation (27). This special property is exact only for the exponential distribution, but since it is exact for any τ_0, it will be approximately true for any monotonic $\rho(\tau)$. As a specific relevant example, we can conclude that for an exponential $\rho(\tau)$, the large-A σN curve is the same (in shape) for seed ^{56}Fe as it is for seed consisting of all Fe, Ni, and Cu isotopes—regardless of the substantial uncertainty in the small ^{58}Fe cross section. The importance of the seed distribution in the case of nonexponential $\rho(\tau)$ can be investigated conveniently with equation (29).

In Figure 9 we summarize the effects of branching on the nuclei between ^{74}Ge and ^{92}Zr for an exponential distribution of exposures. For convenience all σN products are expressed as fractions of that of ^{74}Ge. The figure looks complicated because so much information is displayed, but it can easily be read by first confining one's

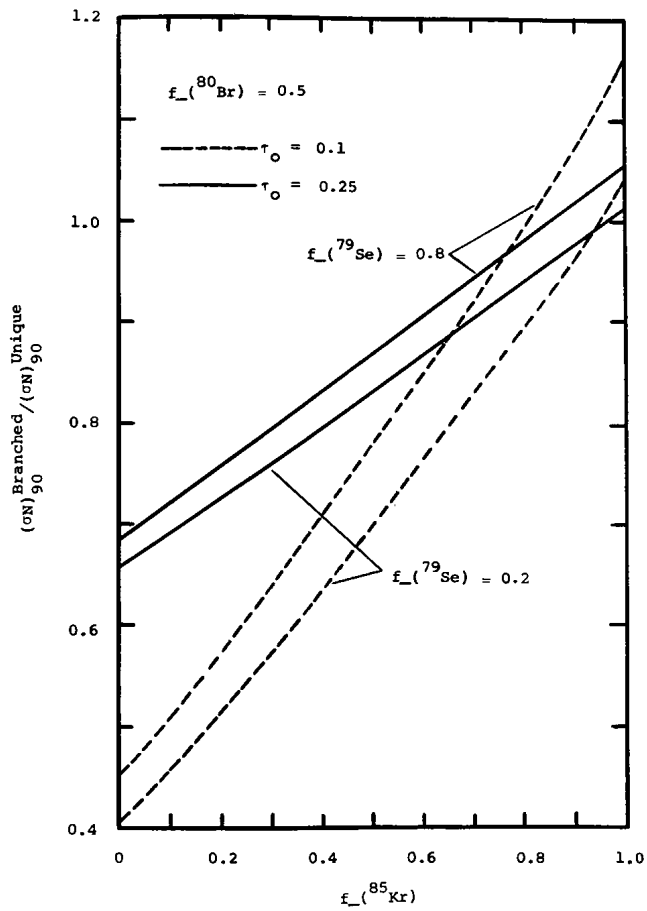

FIG. 7.—The same effect as in Fig. 6 except that ψ_{90} has now been integrated over an exponential exposure distribution for characteristic values of τ_0.

attention to particular choices for the branching parameters. To illustrate large branching effects we choose two very different values of f_- at both of the two major branch points occurring in this region. The sequences generated from $f_-(^{79}\mathrm{Se}) = 0.1$ are connected by a solid line, whereas those generated from $f_-(^{79}\mathrm{Se}) = 0.9$ are connected by a dashed line. The solid points designate the primary isobar at each atomic weight, whereas the open points designate the secondary isobar. The secondary sequences generated by the choices $f_-(^{85}\mathrm{Kr}) = 0.1$ and 0.9 are shown for both choices for $f_-(^{79}\mathrm{Se})$. The other branches occurring in this region have the fixed values $f_-(^{80}\mathrm{Br}) = 0.4$, $f_{ec}(^{81}\mathrm{Kr}) = 0.5$, and $f_-(^{87}\mathrm{Rb}) = 0.1$. The importance of branching is obvious from the large structural differences and from the curious production in certain regions of a positive slope in the σN curve (Stroud 1972).

A monotonic $\rho(\tau)$ must produce a monotonic σN *except* when branching occurs. The choice here of $f_-(^{85}\mathrm{Kr}) = 0.1$ produces a positive slope in the Sr isotopes, which can be understood as follows. The σN of ^{88}Sr dominates because 90 percent of the flow bypasses ^{86,87}Sr in this case, and $(\sigma N)_{87} > (\sigma N)_{86}$ because 10 percent of the major flow through ^{87}Rb has for this example been taken to decay to ^{87}Sr. This result does not match the solar σN values, which are shown as crosses, but it does suggest why their drop is not as steep as the calculation for an unbranched chain, without requiring structure in $\rho(\tau)$ as Clayton (1965) suggested. This result also shows why sophistication is required in determining $(\sigma N)_{87}/(\sigma N)_{86}$ for the method of cosmochronology devised by Clayton (1964). This example should only be taken as illustrative, however, because the average conditions that we will find for the s-process do not suggest that $f_-(^{87}\mathrm{Rb})$ should be as large as the value 0.1 taken for the construction of Figure 9.

IV. APPLICATIONS TO SELECTED BRANCHES

We will now use the formalism that has been developed to study several branches in the s-process synthesis of the solar-system heavy elements. Consistent with our earlier assumptions, all branching will be considered time-independent and a function only of the average thermodynamic environment of the site of the s-process. This requirement of a unique average neutron flux (or neutron density) gives simply that $\lambda_n^i/\lambda_n^j = \sigma_i/\sigma_j$ for any two nuclei along the path. Now for the important negatron-emitting branch points, we therefore have that

$$\frac{t_-^j(T)}{t_-^i(T)} = \left[\frac{1}{f_-^j(T,n_e)} - 1\right] \Big/ \left[\frac{1}{f_-^i(T,n_e)} - 1\right] \frac{\sigma_i(T)}{\sigma_j(T)}, \tag{52}$$

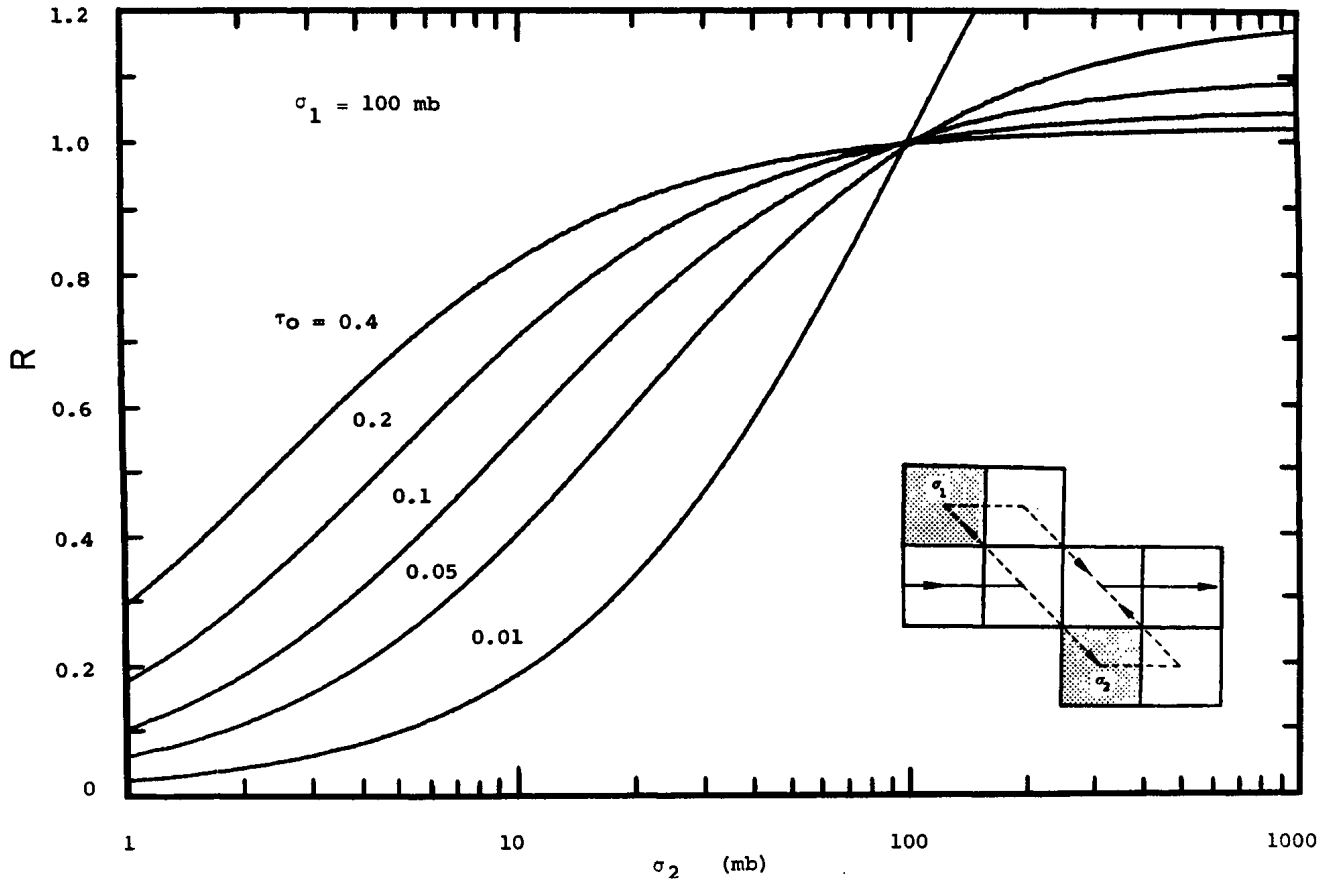

FIG. 8.—The relative-delay effect of alternative capture paths through cross sections of different size. The ratio of σN products beyond the branch is plotted as a function of σ_2 for fixed σ_1 (see inset) and various values of τ_0.

where t_- is the half-life against beta decay, and we have explicitly indicated the temperature and electron-density dependence of all quantities. The branching ratios $f_-^i(T, n_e)$ are determined by fitting observed σN ratios within each branch and are functions of the temperature and free-electron density to the extent that further internal branching (e.g., ^{80}Br in the ^{79}Se branch) also depends on these quantities.

The beta-decay rates used were taken from the calculations of Newman (1973). The principal effects considered were the influence of nuclear excited states (Cameron 1959) and continuum-electron capture (Bahcall 1964). Measured log ft values were used where available; otherwise, the average values (Gleit, Tang, and Coryell 1968), log ft = 5.7 (allowed), 7.5 (first forbidden), 8.5 (first forbidden unique), and 12.1 (second forbidden), were used. Nuclear level information was obtained from Lederer, Hollander, and Perlman (1967) and updated as required by *Nuclear Data Sheets*. The population level of K-shell electrons was calculated in a crude way (Newman 1973, Appendix 1) to allow for treatment of bound capture. Continuum capture dominates at temperatures of interest for all but the heaviest nuclei. Figure 10 shows the pronounced temperature dependence of the half-lives, t_-, for relevant negatron-emitting species along the branched s-process path. In Figure 11 we have further illustrated the important effect on the multiple branch point at ^{64}Cu that was originally considered by CFHZ. The influence of temperature and electron density are seen to cause a considerable departure from the laboratory value of $f_-(^{64}\text{Cu}) = 0.38$.

If the cross sections, abundances, and weak-decay rates were all known with sufficient accuracy to warrant the effort, the locus of allowable T and n_e (and, therefore, neutron density) could be obtained by using equation (52) with all possible pairs of branching nuclei, and then numerically searching over these quantities to find a *self-consistent* set of values that best characterize the average s-process conditions. However, in lieu of that approach, we choose to compare each branch in turn with that at ^{85}Kr. This "normalizing" branch was chosen because it contains no significant internal branches. Therefore, the average temperature and density attendant to the synthesis of nuclide i are taken to be solutions to

$$\frac{t_-^i}{t_-(^{85}\text{Kr})} = \left(\frac{f_-\sigma}{1-f_-}\right)_{^{85}\text{Kr}} \left[\frac{1-f_-(T, n_e)}{f_-(T, n_e)\sigma}\right]_i . \tag{53}$$

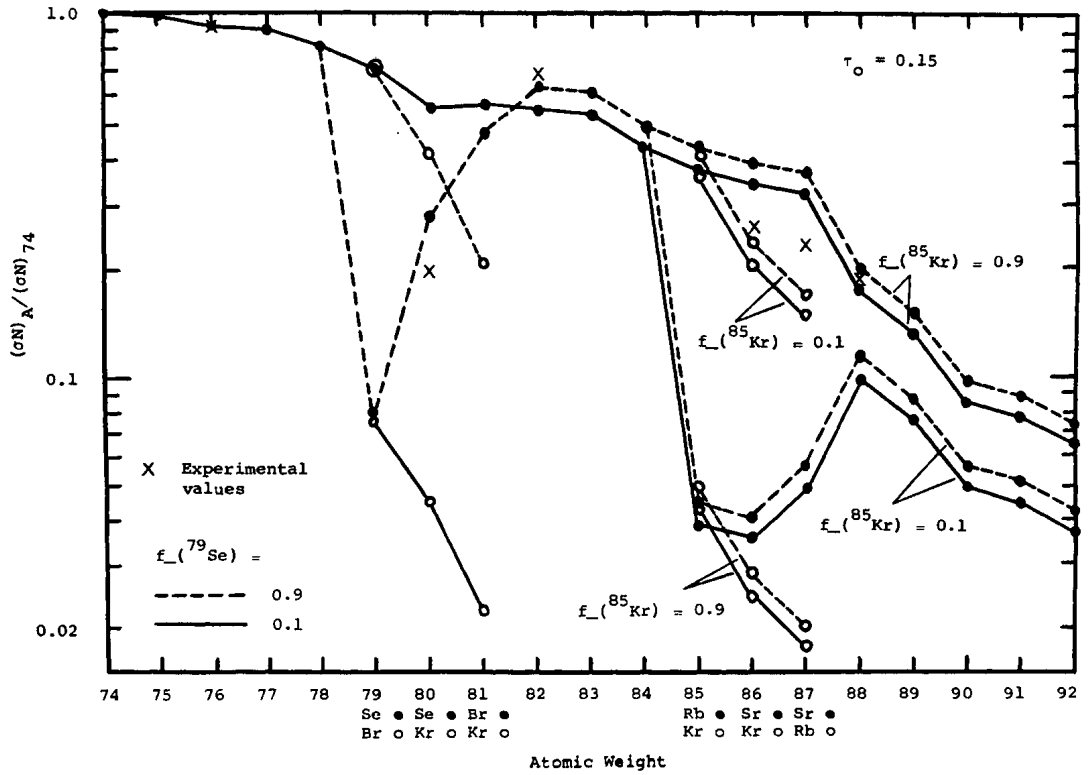

FIG. 9.—The combined effects of the branches at ^{79}Se and ^{85}Kr on the calculated σN curve for a single exponential exposure distribution. The calculated curves have been normalized to $(\sigma N)_{^{74}Ge} = 1.0$. The experimental values have been normalized so that $(\sigma N)_{^{76}Se}$ falls on the calculated curve; the discordant abundance data for the isotopes of Zr (Allen *et al.* 1972) have been omitted. Canonical *s*-process nuclei (*solid points*) and alternate branch members (*open points*) are shown for all possible combinations of the set: $\{f_-(^{79}\text{Se}) = 0.1, 0.9$ and $f_-(^{85}\text{Kr}) = 0.1, 0.9\}$.

Since there are so many uncertainties in all of the input data to such a calculation, one would not expect each branching nucleus to yield exactly the same results. Nevertheless, if the scatter in values is small, we can at least set reasonable bounds on the thermodynamic conditions of solar-system *s*-process nucleosynthesis.

The branching ratios f_- appearing in equation (53) are determined from matching observed σN ratios to those calculated using the formalism of the previous sections. We will restrict most of our attention to forming ratios between primarily *s*-only isotopes of the same element wherever possible (e.g., ^{80}Kr and ^{82}Kr for the branch at ^{79}Se). All abundance data are taken from the compilation of Cameron (1973), and corrections to the abundances of predominantly *s*-process nuclei were made where necessary using interpolations in the empirical *p*- and *r*-process abundance curves. Measured neutron-capture cross sections (at 30 keV) are from Allen, Gibbons, and Macklin (1971) and Stroud (1972). In those many instances where cross sections had to be estimated, we have used the semiempirical values of Allen, Gibbons, and Macklin (where available) combined with the recent Hauser-Feshbach calculations of Holmes and Woosley (1976). When no semiempirical estimates were given, we scaled the calculated results (with a least-squares-type adjustment) to achieve the best consistency with measured cross sections of nearby species. These theoretical cross sections agree quite closely with experiment in most cases, and should be as reliable (within a factor of 2) as the semiempirical estimates.

The results of the experimental σN correlations indicate that the observed distribution can be quite adequately fitted by a superposition of two exponentials characterized by $\tau_0 = 0.1$ for $A \lesssim 75$ and $\tau_0 = 0.25$ for $A \gtrsim 75$. The boundary is not rigid, but does reflect the general need for a more steeply falling $\rho(\tau)$ in the mass region just beyond the iron peak. The major constraints on such exposure distributions are the relatively low observed σN values of ^{58}Fe and ^{59}Co ($\sim 1.2 \times 10^4$ mb and $\sim 7.7 \times 10^4$ mb [Si $\equiv 10^6$], respectively). The maximum allowable *s*-process yield is further limited by the fact that these species are effectively produced in other processes of nucleosynthesis (e.g., Hainebach, Clayton, and Arnett 1974). With this restriction in mind, we find that the maximum ratio of exposed iron seed with $\tau_0 = 0.1$ to that with $\tau_0 = 0.25$ would be limited to only $G_1\tau_{01}/G_2\tau_{02} \sim 4$ (cf. eq. [29]). As a result the exponential $\rho(\tau)$ would be able to account for only a small fraction of the abundances of most of the isotopes of Ni, Cu, and Zn that are on the *s*-process path [unless a sharp cutoff in $\rho(\tau)$ is postulated for small τ]. The advantages of using the exponential form are that (i) the effects of *all* preceding branches divide out when we form σN ratios (*cf.* eq. [27]), enabling us to consider each branch independently; and (ii) the important *non-equilibrium* effects caused by small cross sections in the path are taken into account. This second point is especially

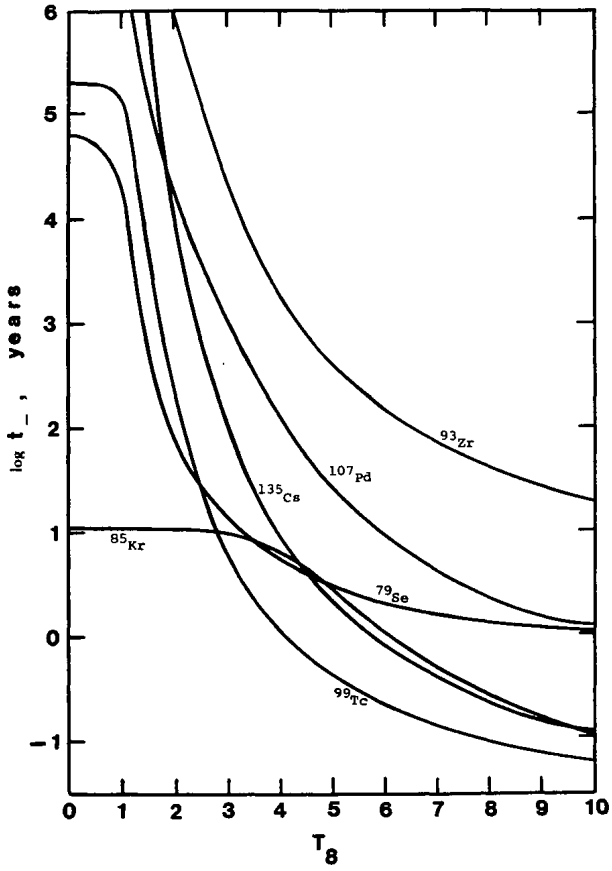

FIG. 10*a*

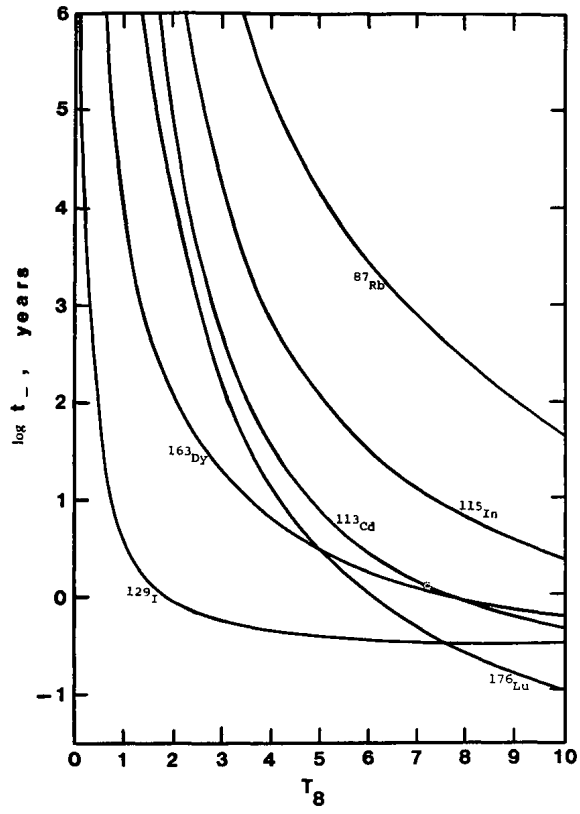

FIG. 10*b*

FIG. 10.—Temperature dependence of the beta-decay half-lives for key negatron-emitting nuclei of importance to *s*-process branching. Note that $T_8 = 10^{-8}T$ K.

significant since the branching systems at ^{63}Ni, ^{79}Se, and ^{85}Kr all occur in a rapidly falling portion of the solar-system σN curve where small cross sections are quite common.

As mentioned previously, a single value of the exponential parameter τ_0 cannot simultaneously produce the rapid increase toward iron and still preserve the level of the observed ledge-precipice behavior for $100 < A < 200$. This large-A region requires a larger value of τ_0 to maintain the relatively flat structure on either side of the drop near the closed shell at 82 neutrons ($A \sim 140$). Seeger, Fowler, and Clayton (1965) pointed out that the exponential $\rho(\tau)$ results from simple remixing models of the Galaxy where the cumulative exposure is just proportional to the number of times the seed nuclei have been processed through a stellar interior. Ulrich (1973) has obtained a completely analogous result for repeated helium-shell flashes in a convective mixing cycle.

We can easily see how the inclusion of convective mixing can quite naturally lead to different values of τ_0. If we simply assume that a fraction, $\mathscr{F}$, of the exposed *s*-process nuclei were convectively removed from the synthesizing region of a star over a mixing time scale, $\mathscr{T}$, then we may rewrite equation (1) as

$$\frac{dN_A}{dt} = n_n\langle\sigma v\rangle_{A-1}N_{A-1} - n_n\langle\sigma v\rangle_A N_A - \frac{\mathscr{F}}{\mathscr{T}}N_A\,. \tag{54}$$

Integrating this equation over $\rho(\tau) = G\exp(-\tau/\tau_0)$ and rearranging, we obtain

$$(\sigma N)_A = \left(1 + \frac{1}{\tau_0\sigma_A} + \frac{\mathscr{F}}{\Phi\mathscr{T}\sigma_A}\right)^{-1}(\sigma N)_{A-1}\,, \tag{55}$$

where $\Phi = n_n v_T$ is the constant neutron flux. From the form of equation (55) we see that the inclusion of repeated mixing episodes yields the same analytical form as the usual exponential results (Clayton and Ward 1974) with the modified exposure parameter

$$\tau_0' = \left(\frac{1}{\tau_0} + \frac{\mathscr{F}}{\Phi\mathscr{T}}\right)^{-1}.$$

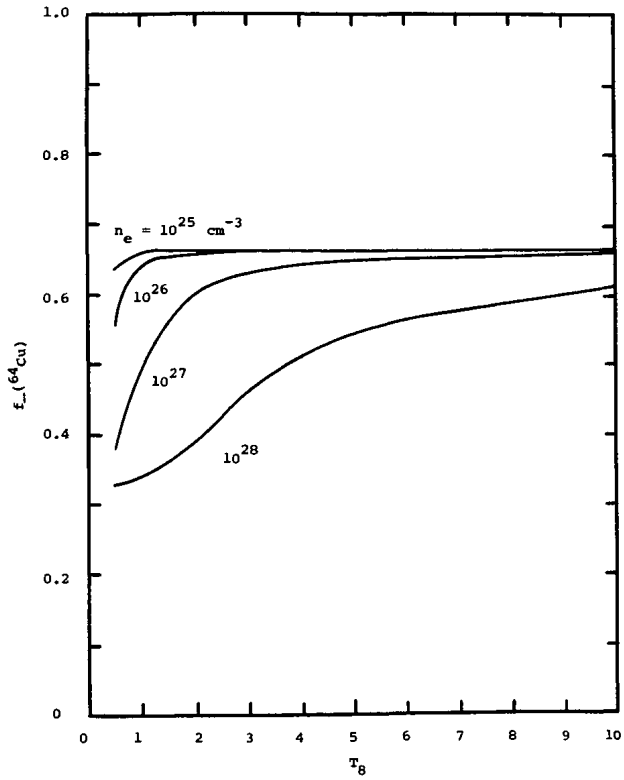

FIG. 11.—Temperature dependence of the β^- branching ratio at ^{64}Cu for various values of the free-electron density. In the laboratory $f_-(^{64}\text{Cu}) = 0.38$.

Thus, by merely varying the flux, mixing fraction, or convective time scale, the stellar environment can quite naturally produce an exponential exposure distribution with a spectrum of values for τ_0. These considerations reinforce our preference for exponential forms of $\rho(\tau)$.

At this point we should note that the cross sections used are valid only for $kT = 30$ keV ($T_8 = 3.5$). However, when forming σN *ratios* as in equation (27), the only noncanceling temperature dependence (assuming all of the cross sections scale similarly) appears in the quantity $\sigma\tau_0$. Clayton (1965) has shown that the integrated fluxes τ_0 that characterize the overall distribution scale as $\tau_0(kT) \approx (kT/30\text{ keV})^{0.7}\tau_0(30\text{ keV})$; since most of the cross sections scale as $T^{-1/2}$, then $\sigma\tau_0 \propto T^{0.2}$, and its temperature dependence is therefore very weak compared to that of the beta-decay rates. However, the anomalous temperature dependence of the smallest, and most important, *s*-process cross sections (e.g., ^{58}Fe, ^{62,64}Ni, ^{88}Sr, ^{138}Ba, and ^{140}Ce) should not be overlooked when sufficient data become available to accurately discern their effects on the σN curve.

Once the proper temperature and branching ratio have been determined, the average neutron density, n_n, and the average flux, Φ, are given by

$$n_n = \frac{\ln 2}{v_T \sigma t_n} = \frac{9.15 \times 10^{10}}{\sigma t_n}\ \text{cm}^{-3}\,, \tag{56}$$

and

$$\Phi = v_T n_n = \frac{1.18 \times 10^{19}\sqrt{T_8}}{\sigma t_n}\ \text{cm}^{-2}\,\text{s}^{-1}\,,$$

with t_n (the half-life against neutron capture) measured in years, σ (the 30 keV cross section) in millibarns, and $T_8 = 10^{-8}\,T$ K, and we have assumed that $\sigma \propto T^{-1/2}$.

One final point must be made for those species where electron capture occurs. Since there does not exist sufficient information at present to independently determine the electron density (as can be done for the temperature), we must somewhat arbitrarily select a value. For a sufficiently high density ($\rho \gtrsim 4.8 \times 10^4\, T_8^{3/2}$ g cm^{-3}), the effects of electron degeneracy in inhibiting negatron emission (Peterson and Tripp 1973) will become significant. In this work, however, we will favor the lower density helium-burning regions ($\rho < 10^4$ g cm^{-3}) and will not consider degeneracy effects. Furthermore, we have followed the work of Weigert (1966), Schwarzschild and Härm (1967), and Iben (1975), and have taken an average density of $\rho = 2000$ g cm^{-3} as characteristic of the helium shell-burning regions undergoing periodic thermal pulses and convective mixing. Therefore, with $\mu_e = 2$ the adopted free-electron density is $n_e = \rho N_0/\mu_e = 6.0 \times 10^{26}$ cm^{-3}.

In the subsections that follow we will consider several key *s*-process branches as indicators of the mean temperature and neutron-capture time scale for the solar-system *s*-process elements. The results of the computations are summarized in Table 1.

a) ^{79}Se

This branch will be considered first in order to illustrate the general technique that was used in our analysis of the other branches. The effects of the stellar environment on the weak-decay rates will yield a quite different result from that originally obtained by Burbidge *et al.* (1957). The decay rate for ^{79}Se is dominated at $T_8 > 1$ by the allowed decay from the low-lying excited state at 96 keV, as emphasized by Cameron (1959). For the internal branch at ^{80}Br, the ground-state β^-, β^+, and electron-capture decays are all allowed. The marked deviation from the laboratory value of $f_-(^{80}\mathrm{Br}) = 0.92$ reflects the effects of continuum-electron capture. There is also competition between electron capture and neutron capture at ^{81}Kr. However, its large estimated cross section ($\sim$450 mb) will not significantly affect the flow through the branch system—although its subsequent decay could have a discernible influence on the abundance of ^{81}Br if the cross sections of ^{81}Kr and ^{81}Br prove to be very different.

Our use of the exponential form of $\rho(\tau)$ throughout this section will make it convenient to define the quantity

$$\zeta(^AZ) \equiv \left[1 + \frac{1}{\tau_0 \sigma(^AZ)}\right]^{-1} . \tag{57}$$

If we now neglect electron capture at ^{81}Kr, then we may explicitly expand equation (27) to obtain the *s*-only ratio:

$$\frac{(\sigma N)_{^{82}\mathrm{Kr}}}{(\sigma N)_{^{80}\mathrm{Kr}}} = \zeta(^{82}\mathrm{Kr})\left[\left[\zeta(^{81}\mathrm{Kr}) + \frac{\zeta(^{81}\mathrm{Br})\zeta(^{80}\mathrm{Se})}{\zeta(^{80}\mathrm{Kr}) f_-(^{80}\mathrm{Br})}\left\{\left[\frac{1}{f_-(^{79}\mathrm{Se})} - 1\right] \Big/ [\zeta(^{79}\mathrm{Br})] + 1 - f_-(^{80}\mathrm{Br})\right\}\right]\right]. \tag{58}$$

Letting $\mathscr{R} \equiv (\sigma N)_{^{82}\mathrm{Kr}}/(\sigma N)_{^{80}\mathrm{Kr}}$ be the observed value, then equation (58) may be inverted to yield

$$\frac{1}{f_-(^{79}\mathrm{Se})} - 1 = f_-(^{80}\mathrm{Br})\zeta(^{79}\mathrm{Br})\left\{\frac{\zeta(^{80}\mathrm{Kr})}{\zeta(^{81}\mathrm{Br})\zeta(^{80}\mathrm{Se})}\left[\frac{\mathscr{R}}{\zeta(^{82}\mathrm{Kr})} - \zeta(^{81}\mathrm{Kr})\right] + 1\right\} - \zeta(^{79}\mathrm{Br}) . \tag{59}$$

Requiring that equation (53) also be satisfied, we have the additional constraint that

$$\frac{1}{f_-(^{79}\mathrm{Se})} - 1 = \left[\frac{1}{f_-(^{85}\mathrm{Kr})} - 1\right]\frac{t_-(^{79}\mathrm{Se})}{t_-(^{85}\mathrm{Kr})}\frac{\sigma(^{79}\mathrm{Se})}{\sigma(^{85}\mathrm{Kr})} . \tag{60}$$

Using the values we will show to result from the ^{85}Kr branch: $f_-(^{85}\mathrm{Kr}) = 0.82$ and $\sigma(^{85}\mathrm{Kr}) = 125$ mb, along with $\sigma(^{79}\mathrm{Se}) = 250$ mb and $\tau_0 = 0.25$, we have plotted the right-hand sides of equations (59) and (60) in Figure 12. The points of intersection show the allowable values of T (for different n_e) required to fit the observations. Note that electron densities much greater than $\sim 3 \times 10^{27}$ cm^{-3} ($\rho \sim 10^4$ g cm^{-3}) would seem to be precluded from producing ^{80}Kr and ^{82}Kr in the correct ratio, thus reinforcing our bias mentioned earlier in favor of a lower density helium-burning environment. With $\rho = 2000$ g cm^{-3} we and that the branching requirements can be met near $T_8 = 2.9$. The figure also indicates that considerably higher values of the temperature are also allowed but require larger neutron densities, since $n_n = 1.6 \times 10^8/t_-(^{85}\mathrm{Kr})$ cm^{-3}, where $t_-(^{85}\mathrm{Kr})$ is in years (as shown in Fig. 10*a*). An additional conclusion can be drawn at this branch about the uncertain absolute Kr abundance.

TABLE 1

SUMMARY OF *s*-PROCESS BRANCHING SOLUTIONS*

Branching Nuclide	σ(mb)	t_β(Lab) (yr)	f_β	T_8	$t_\beta(T_8)$ (yr)	$t_n(T_8)$ (yr)
^{79}Se.....	250	6.5(4)	0.58	2.9	17	23
^{80}Br.....	...	3.4(−5)	0.46	2.9	...	...
^{85}Kr.....	125	1.1(1)	0.82	~3	~10	~46
^{93}Zr.....	70	9.5(5)	0.28	?	...	...
^{113}Cd.....	840	9.0(15)	0.032	3.3	190	6.3
^{134}Cs.....	1000	2.1	0.72	3.4	2.1	5.3
^{151}Sm.....	2500	9.3(1)	0.076	?	<93	<7.6
^{152}Eu.....	...	1.3(1)	0.97	>2	<0.016	...
^{154}Eu.....	4640	8.6	0.83	?	<8.6	<42
^{163}Dy.....	1600†	∞	0.29	~4	~6.3	~2.6
^{163}Ho.....	2820	3.3(1)	0.23	~4	~5.1	~1.5
^{176}Lu.....	2250†	2.6(10)	0.67	?	...	...

* Calculated at $\rho = 2000$ g cm^{-3}. Note that $a(b) \equiv a \times 10^b$.

† Experimental value.

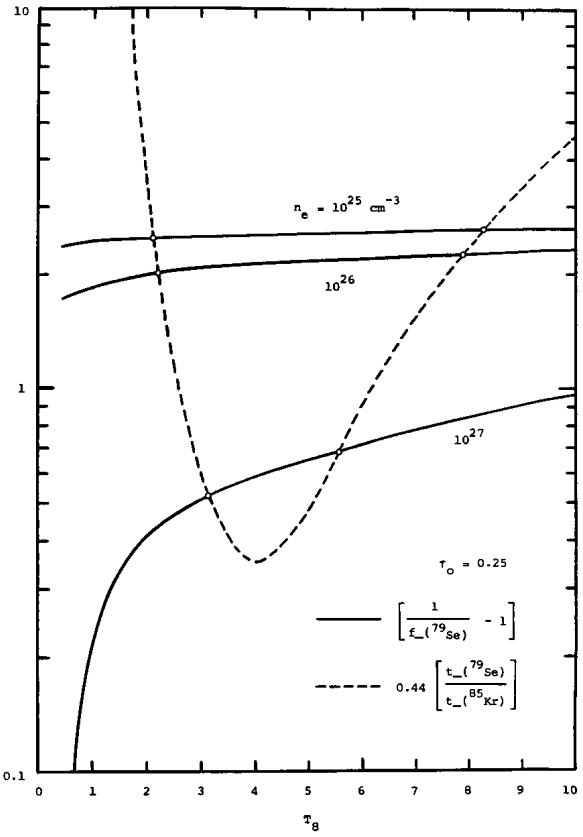

FIG. 12.—Illustration of the technique used to determine the temperature that simultaneously satisfies the branching requirements at ^{79}Se and ^{85}Kr. The intersections of the curves show the allowed temperatures for different values of the electron density.

Since about 80 percent of the measured abundance of ^{80}Se is probably due to the s-process, we also can meaningfully examine

$$\frac{N_s(^{80}\text{Kr})}{N_s(^{80}\text{Se})} \approx \left[\frac{\sigma(^{80}\text{Se}) + (1/\tau_0)}{\sigma(^{80}\text{Kr}) + (1/\tau_0)}\right]\left[\frac{1}{f_-(^{79}\text{Se})f_-(^{80}\text{Br})} - 1\right]^{-1}. \tag{61}$$

Taking the values $f_-(^{79}\text{Se}) = 0.58$, $f_-(^{80}\text{Br}) = 0.46$, and $\tau_0 = 0.25$, we obtain $N_s(^{80}\text{Kr}) = 1.61$—which is in reasonable agreement with Cameron's (1973) interpolated value of 1.06, considering our use of the estimated value $\sigma(^{80}\text{Kr}) = 140$ mb and the large uncertainty in the measured value $\sigma(^{80}\text{Se}) = 20 \pm 12$ mb. If, however, we allow for a sharper r-process peak at ^{80}Se (Seeger, Fowler, and Clayton 1965) and thereby attribute only 57 percent of the abundance of ^{80}Se to the s-process, we obtain much better agreement with s-only ^{76}Se *and* reduce $N_s(^{80}\text{Kr})$ to 1.17.

b) ^{85}Kr

The details of this branch system were given in our discussion in § II. However, the general treatment given there will be simplified to the case where ^{86}Rb always β^- decays and ^{87}Rb always captures a neutron. This latter restriction is temperature-dependent; however, the ground state of ^{87}Rb is third forbidden and the first excited state (403 keV) is second forbidden. An allowed decay is not encountered until the second excited state at 846 keV. Consulting Figure 10*b* shows that the lifetime is long for $T_8 < 8$. The decay of ^{85}Kr is characterized by a first-forbidden ground state, while the first excited state (305 keV) has an allowed decay. Consequently, the half-life remains near its laboratory value (10.8 years) before beginning to decrease for $T_8 \gtrsim 3$.

We may now determine the branching ratio from (cf. eq. [27])

$$\frac{(\sigma N)_{^{88}\text{Sr}}}{(\sigma N)_{^{86}\text{Sr}}} = \zeta(^{88}\text{Sr})\left\{\zeta(^{87}\text{Sr}) + \frac{\zeta(^{86}\text{Kr})\zeta(^{87}\text{Rb})}{\zeta(^{85}\text{Rb})\zeta(^{86}\text{Sr})}\left[\frac{1}{f_-(^{85}\text{Kr})} - 1\right]\right\}. \tag{62}$$

Simply inverting the above expression, we find that $f_-(^{85}\text{Kr}) = 0.82$, using Cameron's (1973) abundances and attributing at least 80 percent of the ^{88}Sr abundance to the s-process. This result was obtained by taking the Allen,

Gibbons, and Macklin estimate $\sigma(^{86}\mathrm{Kr}) = 9$ mb. It is important to note that the observed value for the left-hand side of equation (62) is < 1 and could therefore not be explained by any branching calculations using the steady-flow approximation [which would require $(\sigma N)_{^{86}\mathrm{Sr}} < (\sigma N)_{^{88}\mathrm{Sr}}$]. The pronounced deviation from steady flow is caused by the small cross sections at ^{86}Kr and ^{88}Sr. If the value of $\sigma(^{86}\mathrm{Kr})$ is smaller than the one used (Holmes and Woosley calculate 4.2 mb), then the branching ratio would be correspondingly lower. With this in mind we may examine the extent to which ^{86}Kr is produced in the *s*-process by using

$$N_s(^{86}\mathrm{Kr}) = \frac{\zeta(^{84}\mathrm{Kr})\zeta(^{83}\mathrm{Kr})}{[\sigma(^{86}\mathrm{Kr}) + (1/\tau_0)]}\,(\sigma N)_{^{82}\mathrm{Kr}}\left[\frac{1}{1 - f_-(^{85}\mathrm{Kr})} + \frac{1}{\tau_0\sigma(^{85}\mathrm{Kr})}\right]^{-1}. \tag{63}$$

Taking $\sigma(^{85}\mathrm{Kr}) = 125$ mb, $f_-(^{85}\mathrm{Kr}) = 0.82$, and correcting the abundance of ^{82}Kr with that of *p*-only ^{78}Kr gives $N_s(^{86}\mathrm{Kr}) = 5.05$, thereby giving an *r*-process contribution of 3.08. This low *r*-process yield indicates that the extrapolated *r*-process curve of Cameron (1973) should be revised downward substantially between ^{82}Se and ^{100}Mo (Seeger, Fowler, and Clayton 1965). With such an interpretation for the branching at ^{85}Kr we also find that the abundance of ^{87}Rb is primarily due to the *s*-process. The only drawback is that with the factor of ~ 2 decrease in the Sr abundance from 1968 to 1973, Sr is now overproduced by just about this same amount. The measurement of the cross sections for the isotopes of Kr would, of course, refine all of these arguments considerably.

c) ^{93}Zr

Consideration of this possible branch is motivated by the recent *p*-process calculations of Audouze and Truran (1975) which were unable to produce a sufficient amount of ^{94}Mo to account for its observed abundance. A branch in the *s*-process can meet the requirement, providing that the decay of ^{94}Nb is fast enough. Although the half-life of ^{94}Nb in the laboratory is 2×10^4 years (second forbidden decay), the very low-lying first excited state at only 41 keV has an allowed decay; so for $T_8 > 2$, the half-life is short ($\ll 1$ year). Thus a branch at ^{93}Zr quite naturally leads to some production of ^{94}Mo by the *s*-process with

$$f_-(^{93}\mathrm{Zr}) = \left\{\frac{\zeta(^{94}\mathrm{Mo})\zeta(^{93}\mathrm{Nb})}{\zeta(^{94}\mathrm{Zr})}\left[\frac{(\sigma N)_{^{96}\mathrm{Mo}}}{\zeta(^{96}\mathrm{Mo})\zeta(^{95}\mathrm{Mo})(\sigma N)_{^{94}\mathrm{Mo}}} - 1\right] + 1\right\}^{-1}. \tag{64}$$

Requiring all of the observed amount of ^{94}Mo to be produced relative to *s*-only ^{96}Mo gives $f_-(^{93}\mathrm{Zr}) = 0.46$; if we reduce the yield to only 50 percent of ^{94}Mo then $f_-(^{93}\mathrm{Zr}) = 0.22$.

Further information on the branching ratio can be obtained by considering ^{92}Zr and ^{94}Zr. Although the absolute abundance of Zr is anomalously high relative to the calculated σN curve (Allen, Gibbons, and Macklin 1971; Amiet and Zeh 1968), the predominately *s*-process ratio $N(^{92}\mathrm{Zr})/N(^{94}\mathrm{Zr}) = 0.98$ should survive any scaling and nearly equal small *r*-process corrections. The corresponding branching ratio is

$$f_-(^{93}\mathrm{Zr}) = 1 - \left[\zeta(^{94}\mathrm{Zr})\frac{(\sigma N)_{^{92}\mathrm{Zr}}}{(\sigma N)_{^{94}\mathrm{Zr}}} - \frac{1}{\tau_0\sigma(^{93}\mathrm{Zr})}\right]^{-1}. \tag{65}$$

With the estimate $\sigma(^{93}\mathrm{Zr}) = 70$ mb we find $f_-(^{93}\mathrm{Zr}) = 0.28$. This result is in general agreement with the range derived earlier from the Mo isotopes. If we take the σN level in this mass region to be ~ 90 mb (Si $\equiv 10^6$), then $f_-(^{93}\mathrm{Zr}) = 0.28$ gives an *s*-process contribution to ^{93}Nb of ~ 1 (after the decay of ^{93}Zr). The resulting low *r*-process yield of ~ 0.4 is then consistent with the lower trend in the *r*-process curve discussed for the branch at ^{85}Kr, and also results in good agreement of ^{96}Zr with *r*-only ^{100}Mo *if* the Zr abundance is reduced by a factor of ~ 1.6.

The only difficulty with the above requirements on $f_-(^{93}\mathrm{Zr})$ is caused by the slow decay of ^{93}Zr. The ground-state transition is second forbidden, and it appears that the known excited states are at least first forbidden. Thus the decrease in the half-life with increasing temperature is slow (*cf.* Fig. 10*a*). Use of the calculated half-life then requires neutron densities much lower and temperatures much higher than are indicated for the other branches. The situation can not be remedied by lowering the cross section of ^{93}Zr because too much ^{93}Nb would then result. The apparent cure would be for some of the excited-state decays to have log *ft* values somewhat smaller than our estimates.

d) ^{113}Cd

Special consideration of this branch point is again dictated by the results of Audouze and Truran (1975), which indicate a severe underproduction of ^{113}In in their *p*-process calculations. To examine the production of ^{113}In by a branch in the *s*-process path at ^{113}Cd, we will first consider the important beta-active species in this region. Although the ground state of ^{113}Cd is fourth forbidden, the first excited state at 270 keV is only first forbidden and result in a dramatic decrease in the half-life at *s*-process temperatures (Fig. 10*b*). For ^{114}In the ground-state decays are all allowed and fairly rapid. The principal temperature dependence is from continuum-electron capture for $T_8 > 2$; the net effect of the stellar environment is to give $f_-(^{114}\mathrm{In}) = 1$. The major point to note from the ^{114}In

decay is that any s-process production of ^{113}In will also necessarily result in a contribution to ^{114}Sn and ^{115}Sn. Finally, for ^{115}In the ground-state decay is highly forbidden, but the first excited state (allowed decay) is fairly high in energy (335 keV), and the half-life remains long until $T_8 > 7$.

To proceed with the calculation, we will take the σN level of s-only ^{116}Sn as 50 mb (Si $\equiv 10^6$). Neglecting the beta decay of ^{115}In, we have

$$N_s(^{113}\text{In}) = \frac{(\sigma N)_{^{116}\text{Sn}}}{\sigma(^{113}\text{In})\zeta(^{116}\text{Sn})}\left\{\zeta(^{115}\text{Sn})\zeta(^{114}\text{Sn}) + \zeta(^{114}\text{Cd})\zeta(^{115}\text{In})\left[\frac{1}{f_-(^{113}\text{Cd})} - 1\right]\Big/[\zeta(^{113}\text{In})]\right\}^{-1}. \quad (66)$$

The results for ^{114}Sn and ^{115}Sn can then be calculated recursively from this result. Using the usual value $\tau_0 = 0.25$ and supplementing the Allen, Gibbons, and Macklin estimates with $\sigma(^{113}\text{Cd}) = 840$ mb, we find that all of the abundance of ^{113}In can be produced with $f_-(^{113}\text{Cd}) = 0.032$. We also, therefore, produce 56 percent of the observed amount of ^{114}Sn and 25 percent of ^{115}Sn. Requiring that equation (53) be satisfied for consistency with the other branches, we find that the correct branching ratio is produced at $T_8 = 3.3$. In this case we may draw the additional conclusion that to avoid a factor of 2, say, overproduction of ^{113}In, ^{113}Cd could not have remained at this temperature in the *absence* of a neutron flux for >700 years. If we lower the temperature to $T_8 = 3$, then the following s-process production results: 51 percent of ^{113}In, 28 percent of ^{114}Sn, and 12 percent of ^{115}Sn. This branch also serves to place an upper limit on the mean s-process temperature, since taking $T_8 = 4$ results in ^{113}In being *overproduced* by a factor of 3.8 and ^{114}Sn by a factor of 2.

e) ^{134}Cs

The cross section of s-only ^{136}Ba has recently been measured (Stroud 1972) as 90 ± 20 mb and gives excellent agreement with the fit of an exponential exposure distribution through the s-only isotopes of Mo, Cd, Sn, Te, and Sm that have measured cross sections. As a result, if we take the adjusted calculated value (Holmes and Woosley 1976) of $\sigma(^{134}\text{Ba}) = 200$ mb, we find that a branch at ^{134}Cs is needed to explain the s-only ratio $(\sigma N)_{^{134}\text{Ba}}/(\sigma N)_{^{136}\text{Ba}} < 1$. We note that our adopted value for $\sigma(^{134}\text{Ba})$ is higher than the 155 mb estimate of Allen, Gibbons, and Macklin, since their estimate for $\sigma(^{136}\text{Ba})$ was too low at 37 mb. The other cross section that is needed for this branch is that of ^{134}Cs. Since $\sigma(^{133}\text{Cs})$ is measured as 700 ± 40 mb, the odd-odd nucleus ^{134}Cs should have a larger cross section, and we will adopt $\sigma(^{134}\text{Cs}) = 1000$ mb.

The ground-state decay of ^{134}Cs undergoes two allowed transitions, so it seems reasonable to assume that the effects of the excited states would not appreciably reduce its laboratory half-life of 2.06 years. For ^{135}Cs, however, the first excited state at 250 keV has an allowed transition (compared with a second forbidden ground state) and gives a marked decrease in the effective half-life, as shown in Figure 10*a*. The correct branching ratios will then be solutions to

$$\frac{(\sigma N)_{^{136}\text{Ba}}}{(\sigma N)_{^{134}\text{Ba}}} = \zeta(^{136}\text{Ba})\left[\left[\frac{\zeta(^{135}\text{Ba})\zeta(^{134}\text{Ba})}{1/[f_-(^{134}\text{Cs})] - 1} + \left\{1 + \frac{\zeta(^{135}\text{Ba})}{1/[f_-(^{135}\text{Cs})] - 1}\right\}\Big/\left[\frac{1}{1 - f_-(^{135}\text{Cs})} + \frac{1}{\tau_0\sigma(^{135}\text{Cs})}\right]\right]\right.$$
$$\left.\times\left\{\frac{\sigma(^{134}\text{Ba})}{\sigma(^{136}\text{Ba})} + \frac{\zeta(^{134}\text{Ba})}{1/[f_-(^{134}\text{Cs})] - 1}\right\}^{-1}, \quad (67)$$

where we have included the decay of ^{134}Cs after termination of the neutron flux. Solving equation (67) gives $f_-(^{134}\text{Cs}) = 0.72$; this result is virtually independent of $f_-(^{135}\text{Cs})$ since the estimated values, $\sigma(^{135}\text{Ba}) = 470$ mb and $\sigma(^{135}\text{Cs}) = 200$ mb, are large enough (for $\tau_0 = 0.25$) to produce only a small differential effect on ^{136}Ba. Assuming that the half-life of ^{134}Cs is independent of temperature, then use of equation (53) gives consistency with the other branches near $T_8 = 3.4$. Any decrease in the effective half-life of ^{134}Cs will yield a correspondingly lower temperature. In contrast to the interpretation of Amiet and Zeh (1968), we see that the peaked structure in the observed σN curve through the isotopes of barium can quite naturally be explained as a combined effect of the branch at ^{134}Cs (producing a positive slope from ^{134}Ba to ^{136}Ba) and the beginning of the precipice (negative slope from ^{136}Ba to ^{138}Ba) due to the small cross section at neutron-magic ^{138}Ba.

f) *The Rare Earths and Beyond*

The importance of branching through the rare earths (beyond the closed shell at 82 neutrons) and on to larger atomic weights is influenced by the absolute level of the unbranched σN curve in this region. Since most of the cross sections are ~1000 mb, the curve for unbranched portions of the path should be relatively flat, the "local approximation" being quite adequate. The two s-only species ^{148}Sm and ^{150}Sm are in good agreement with the earlier s-only isotopes (e.g. ^{136}Ba) and the calculated exponential σN curve which defines the extent of the precipice at $A \sim 140$. Furthermore, they have well-measured cross sections (±20 percent), are not in a branched portion of the path, and so would seem to be the obvious indicators of the s-process yield through the rare earths. With suitable empirical p-process corrections, we have $(\sigma N)_{^{148}\text{Sm}} = 6.1$ mb and $(\sigma N)_{^{150}\text{Sm}} = 5.9$ mb (Si $\equiv 10^6$). The large cross sections in this mass region also allow greater opportunity for branching. If we take the average neutron density

as 1.6×10^7 cm^{-3}, then the half-life of a given species against neutron capture is $t_n \approx 5700/\sigma$ years, with σ in mb at 30 keV. Thus beta-active species with large enough cross sections and half-lives on the order of a year could be expected to cause the σN value for certain nuclei to be lower than the calculated level *if* the cross section of the daughter is substantially smaller than that of its unstable progenitor. Crucial experimental data needed to accurately assess this possibility would be provided by the much-needed measurements of the capture cross sections for ^{152,154}Gd, ^{160}Dy, ^{170}Yb, ^{186}Os, ^{192}Pt, and ^{198}Hg. Use of averages of the estimates of Allen, Gibbons, and Macklin and the calculations of Holmes and Woosley indicate that all of these species except ^{198}Hg lie somewhat below the average calculated σN level. The *overabundance* of ^{198}Hg has been discussed by Blake and Schramm (1973) as possibly being due to postevent neutron exposure of the *r*-process abundance peak at $A \sim 195$. In what follows we will consider only the most secure branches for $A > 140$.

i) ^{151}Sm

This branch is the second *s*-process time-scale indicator originally considered by Burbidge *et al.* (1957). Unfortunately the nuclear physics needed for this system is still very incomplete. The spins of the excited states of ^{151}Sm are not known at present, and only the energy of the first excited state at 68 keV has been measured for ^{154}Eu. This precludes explicit calculations of the temperature dependence of the beta-decay rates, although it seems likely that a reduction in the effective half-lives could be expected. With these difficulties in mind, we will consider the influence of $f_-(^{151}\text{Sm})$, $f_-(^{152}\text{Eu})$, and $f_-(^{154}\text{Eu})$ on the nuclei ^{152}Gd and ^{154}Gd which are shielded from production by the *r*-process. The decay of ^{152}Eu is particularly interesting in that it shows how significantly the effects of the stellar environment can alter the measured laboratory values. So many levels of ^{152}Gd and ^{152}Sm are accessible that several allowed decays occur from the ground and excited states. If log *ft* values for some of the excited-state decays are near the average for allowed decays, t_- may be quite short at temperatures of interest. Figure 13 illustrates these dramatic effects. The electron-capture rate is dominated by continuum capture for $T_8 > 2$ and results in the prominence of the negatron-emission branch, in contrast to its laboratory value of 0.28. Consistent with $\rho = 2000$ g cm^{-3} and for $T_8 > 2$, we take $f_-(^{152}\text{Eu}) = 0.97$. Although significant competition can occur between neutron capture and electron capture at ^{153}Gd, the necessarily small amount of flow that passes through ^{152}Gd will render this complication unwarranted at present.

Our branching arguments in this particular case will be somewhat sensitive to values used for the unmeasured cross section of ^{152}Gd and ^{154}Gd, since there are factor of 2 differences between the estimates of Allen, Gibbons, and Macklin and the calculations of Holmes and Woosley. There is good agreement, however, with the adjusted calculated values: $\sigma(^{151}\text{Sm}) = 2500$ mb (based on ^{150}Sm and ^{152}Sm) and $\sigma(^{154}\text{Eu}) = 4640$ mb (based on ^{151}Eu

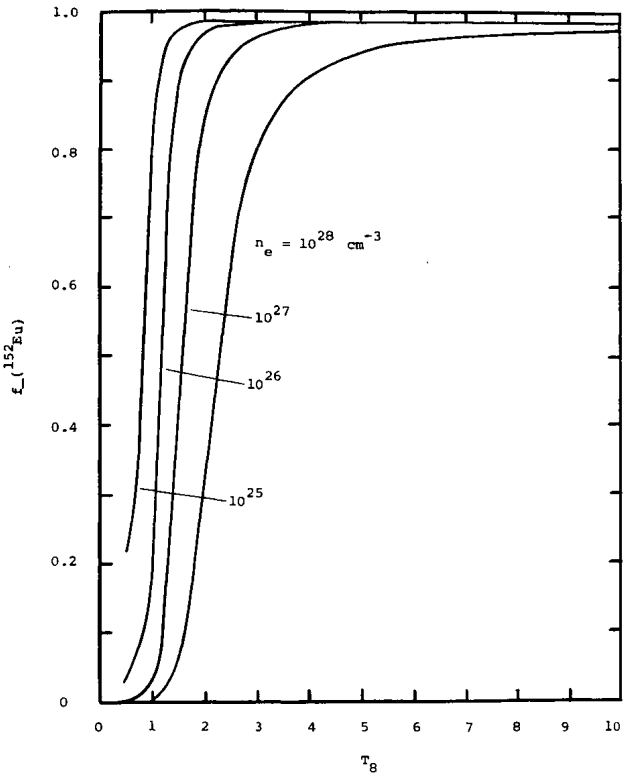

FIG. 13.—Temperature dependence of $f_-(^{152}\text{Eu})$. The laboratory value is 0.28.

and ^{153}Eu). Furthermore, we will take the average s-process yield in this region to be $\langle\sigma N\rangle = 6$ mb (Si $\equiv 10^6$). Postponing inserting numerical values for the uncertain cross sections, production of *all* of ^{152}Gd and ^{154}Gd by the s-process requires that the branching ratios satisfy

$$f_-(^{151}\mathrm{Sm}) = \frac{(\sigma N)_{^{152}\mathrm{Gd}}}{f_-(^{152}\mathrm{Eu})\langle\sigma N\rangle} = \sigma(^{152}\mathrm{Gd})/(9.80 \times 10^3)\,, \tag{68}$$

and

$$f_-(^{154}\mathrm{Eu}) = \left[\frac{N_s(^{154}\mathrm{Gd})}{\langle\sigma N\rangle} - \frac{1}{\sigma(^{154}\mathrm{Eu})}\right]\Big/\left[\frac{1}{\sigma(^{154}\mathrm{Gd})} - \frac{1}{\sigma(^{154}\mathrm{Eu})}\right] = 3.94\left[\frac{4640}{\sigma(^{154}\mathrm{Gd})} - 1\right]^{-1}, \tag{69}$$

where we have included the subsequent decay of ^{154}Eu to ^{154}Gd after the s-process event. The above equations constitute an important pair that must be satisfied in this mass region. Note in particular that equation (69) requires $\sigma(^{154}\mathrm{Gd}) \leq 940$ mb. If we use the estimates of Allen, Gibbons, and Macklin, we find $f_-(^{151}\mathrm{Sm}) = 0.051$ and $f_-(^{154}\mathrm{Eu}) = 0.50$; the calculated values of Holmes and Woosley yield $f_-(^{151}\mathrm{Sm}) = 0.010$ and $f_-(^{154}\mathrm{Eu}) = 1.21$, an unphysical value. Taking a simple average of the estimated cross sections, we find $f_-(^{151}\mathrm{Sm}) = 0.076$ and $f_-(^{154}\mathrm{Eu}) = 0.83$. If we now take the 8.6 yr ground-state half-life of ^{154}Eu, we find that equation (53) cannot be satisfied (and ^{154}Gd is, therefore, severely underproduced) with the average values given above. Furthermore, our average conditions require that $n_n \gtrsim 1.5 \times 10^7$ cm^{-3}; so using the laboratory half-life of ^{151}Sm gives $[f_-(^{151}\mathrm{Sm})]_{\max} = 0.026$ and a maximum s-process yield of 34 percent of ^{152}Gd.

The difficulty can be further emphasized (even if we ignore consistency with the other branches) by merely noting that when we use the *ground-state* half-lives, then $f_-(^{154}\mathrm{Eu}) \geq 0.5$ requires that $f_-(^{151}\mathrm{Sm}) \geq 0.15$, and thus overproduces ^{152}Gd by at least a factor of 3. Although these arguments depend on estimated cross-section values, the low degree of relative fractionation between the rare earths (Mason 1971) and the general requirements for $f_-(^{154}\mathrm{Eu})$ and $f_-(^{151}\mathrm{Sm})$ indicate that the resolution to this problem is that both ^{154}Eu and ^{151}Sm probably have shorter effective half-lives due to more favored decays from the yet-to-be-measured properties of their excited states.

ii) ^{163}Dy

The purpose of this proposed branch will be to attempt to account for the anomalously high abundance of ^{164}Er, which is shielded from production by the r-process and is an order of magnitude more abundant than other p-process nuclei in this mass region. Although the ground state of ^{163}Dy is *stable* in the laboratory, at the elevated temperatures of the stellar interior it can easily decay to ^{163}Ho from its thermally populated excited states (Cameron 1959) due to the very small ($\sim$10 keV) mass difference between them. The 33 year (laboratory) half-life of ^{163}Ho could then allow it to capture a neutron and subsequently form ^{164}Er following the fast beta decay of ^{164}Ho. Although $f_-(^{164}\mathrm{Ho})$ is measured to be 0.40 in the laboratory, the effects of continuum capture and ionization of the K-shell electrons greatly enhance the β^- branch and give $f_-(^{164}\mathrm{Ho}) = 1$ at relevant temperatures and densities.

This explanation is, however, complicated somewhat by the fact that the electron-capture rate of ^{163}Ho will oppose the β^- rate of ^{163}Dy. The excited states of ^{163}Dy at 75 keV and 170 keV both have allowed decays; the return electron capture is also allowed and is dominated by continuum capture above $T_8 \approx 2$. If we use the "local approximation," we then have

$$\frac{(\sigma N)_{^{164}\mathrm{Er}}}{\langle\sigma N\rangle} = \left\{1 + \left[\frac{1}{f_-(^{163}\mathrm{Dy})} - 1\right]\Big/[1 - f_{\mathrm{ec}}(^{163}\mathrm{Ho})]\right\}^{-1}, \tag{70}$$

where $\langle\sigma N\rangle$ is the average level of s-process production in this mass region, and the branching ratios are defined as usual. We also find that

$$f_{\mathrm{ec}}(^{163}\mathrm{Ho}) = \left\{1 + \frac{t_{\mathrm{ec}}(^{163}\mathrm{Ho})}{t_-(^{163}\mathrm{Dy})}\frac{\sigma(^{163}\mathrm{Ho})}{\sigma(^{163}\mathrm{Dy})}\left[\frac{1}{f_-(^{163}\mathrm{Dy})} - 1\right]\right\}^{-1}. \tag{71}$$

Requiring in addition that equation (53) be satisfied for consistency with the other branches, we find that the fraction $f_s(^{164}\mathrm{Er})$ of the abundance of ^{164}Er that can be made by the average s-process is numerically

$$f_s(^{164}\mathrm{Er}) = 1.95\left\{1 + t_-(^{163}\mathrm{Dy})\left[\frac{2.81}{t_-(^{85}\mathrm{Kr})} + \frac{0.57}{t_{\mathrm{ec}}(^{163}\mathrm{Ho})}\right]\right\}^{-1}, \tag{72}$$

where we have taken $\sigma(^{163}\mathrm{Ho}) = 2820$ mb, $\sigma(^{164}\mathrm{Er}) = 875$ mb, $\langle\sigma N\rangle = 6$ mb (Si $\equiv 10^6$), and the values for the ^{85}Kr branch parameters given previously. In Figure 14 we have shown $f_s(^{164}\mathrm{Er})$ as a function of temperature, with the weak-decay rates taken from Newman (1973). From the figure we see that the maximum value is $f_s(^{164}\mathrm{Er}) = 0.56$ at $T_8 = 4$, and that at $T_8 = 3$ (and $\rho = 2000$ g cm^{-3}), $f_s(^{164}\mathrm{Er}) = 0.22$. Apparently, the p-process must be responsible for at least half of the observed amount of ^{164}Er under average s-process conditions.

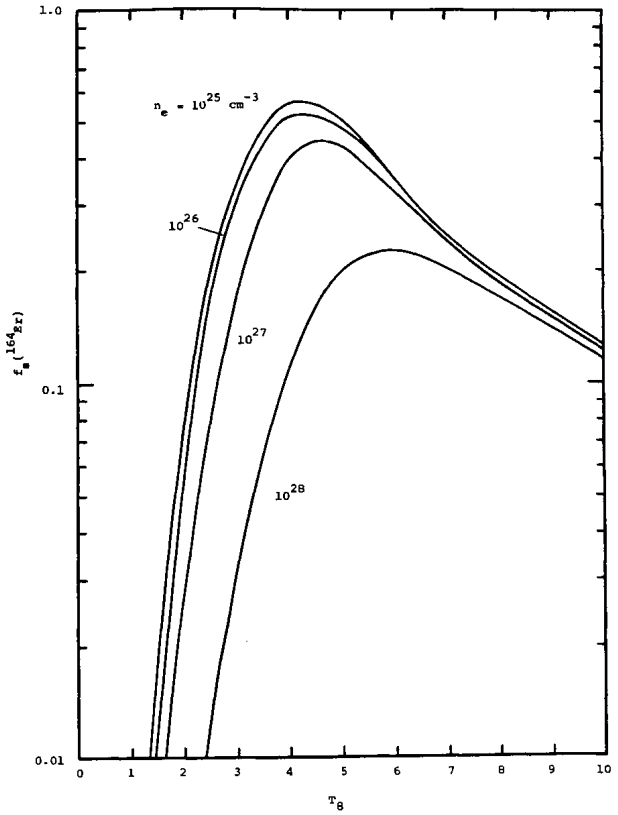

FIG. 14.—The fraction of the observed abundance of ^{164}Er that can be made in the average thermodynamic environment of the *s*-process.

iii) ^{176}Lu

The ^{176}Lu/^{176}Hf pair is somewhat difficult to fit into our average *s*-process branching scheme. Both nuclei are shielded from *r*-process production, and the experimental values (uncorrected for *p*-process contributions or the cosmic decay of ^{176}Lu) are $(\sigma N)_{^{176}\mathrm{Lu}} = 2.42$ mb and $(\sigma N)_{^{176}\mathrm{Hf}} = 6.97$ mb (Si $\equiv 10^6$). Although the combined σN level of 9.39 mb is somewhat above our assumed average level of ~ 6 mb (Si $\equiv 10^6$), we may still derive some information on $f_-(^{176}\mathrm{Lu})$. The temperature dependence of the β^- half-life of ^{176}Lu is shown in Figure 10*b*. The ground state is highly forbidden, as is the first excited state. The effects of the second excited state at 290 keV (first forbidden) are the most dominant. Therefore, if the usual branching had occured at ^{176}Lu, we would have simply

$$f_-(^{176}\mathrm{Lu}) = \left[1 + \frac{(\sigma N)_{^{176}\mathrm{Lu}}}{(\sigma N)_{^{176}\mathrm{Hf}}}\right]^{-1} = 0.74\,, \tag{73a}$$

or

$$f_-(^{176}\mathrm{Lu}) = 1 - \frac{(\sigma N)_{^{176}\mathrm{Lu}}}{\langle \sigma N \rangle} = 0.60\,. \tag{73b}$$

This yields an average branching ratio of 0.67, which agrees with that obtained by Audouze, Fowler, and Schramm (1972). We should note that our lowering of the Zr abundance (discussed earlier), combined with the well-determined Zr/Hf abundance ratio (Mason 1971), would imply a similar lowering (by a factor of ~ 1.6) of the ^{176}Hf abundance (Suess and Zeh 1973); equation (73a) would then yield a more consistent value of 0.64. The essential complication at this point is the interpretation of $f_-(^{176}\mathrm{Lu})$. With the relatively slow decrease in the ^{176}Lu half-life we find that a *much* lower neutron density (or much higher temperature) is required here than at the other branches. Therefore, at our average *s*-process conditions ^{176}Hf will be essentially bypassed.

Instead of identifying $f_-(^{176}\mathrm{Lu})$ with the competition between neutron capture and thermal beta decay, Audouze, Fowler, and Schramm proposed a branch in the capture mechanism itself whereby a fraction of the neutron flow was captured into the 3.7 hour (290 keV) isomeric state of ^{176}Lu, which then decayed directly to ^{176}Hf. Our assumption throughout this work, however, has been that the hot photon bath and inelastic-scattering processes in the stellar interior would always establish thermal equilibrium among the nuclear excited states on a time scale

much shorter than any beta-decay half-lives. This point was emphasized by Clayton and Rassbach (1967) in their discussion of the 3×10^6 yr (α-decaying) isomeric state of ^{210}Bi. It remains to be calculated just how effective de-excitation (Shaw and Clayton 1967; Truran and Kozlovsky 1969) of all such isomeric states (in a hot α-particle environment) can be. There are many other interesting points along the *s*-process path where such a *nonthermal* interpretation of the branching ratios could be important (*including* the key branch at ^{85}Kr).

V. DISCUSSION

The results of the preceding calculations are summarized in Table 1, where for each branching nuclide we have listed (where relevant) (i) the 30 keV neutron-capture cross section (estimates for the unmeasured values were made as discussed earlier in § IV), (ii) the laboratory half-life, (iii) the calculated branching ratio, (iv) the temperature T_8 required for consistency with the branch at ^{85}Kr, (v) the beta-decay half-life at temperature T_8, and (vi) the resulting neutron-capture half-life. Although much of our analysis has depended on the values of estimated cross sections and weak-decay properties of nuclear excited states, a surprisingly consistent picture has developed for an average *s*-process environment characterized by conditions near $T_8 \approx 3.1$ and $n_n \approx 1.6 \times 10^7$ cm^{-3} (with $\rho = 2000$ g cm^{-3}), the resulting neutron flux being $\Phi \approx 3.5 \times 10^{15}$ cm^{-2} s^{-1}. These values are to be compared with the recent results of Ulrich (1973), $T_8 = 2.5$ and $\Phi = 6.3 \times 10^{16}$ cm^{-2} s^{-1}; of Peterson and Tripp (1973), $\Phi \approx 1.2 \times 10^{16}$ cm^{-2} s^{-1}; and of Blake and Schramm (1975), $\Phi \approx 10^{15}$–10^{16} cm^{-2} s^{-1}. The above ranges in temperature and neutron flux would seem to favor such neutron-producing sources as ^{13}C(α, n)^{16}O, ^{17}O(α, n) ^{20}Ne, and ^{22}Ne(α, n) ^{25}Mg. All of these are operative in the range $T_8 = 1$–4 (Reeves 1966 and Clayton 1968), thus reinforcing the location of the *s*-process in the helium shell-burning phase of highly evolved stars (Sanders 1967; Ulrich 1973; Iben 1975). These conditions are in marked contrast to the early estimates of Cameron (1959), $T_8 = 7$ (characteristic of carbon burning) and $\Phi \approx 3 \times 10^{17}$ cm^{-2} s^{-1}.

The species shown in Table 2 are other interesting branch points for which no independent calculations could be made, so we have used the mean values for the temperature and neutron density given above to compute their branching parameters (in the same format as Table 1). We will comment only briefly on three of these: (i) If the *s*-process is responsible for the same *fractional* contribution to the observed abundances of ^{63}Cu and ^{65}Cu, then for $\tau_0 = 0.1$ the branch at ^{63}Ni (and ^{64}Cu) independently yields values for the temperature and neutron density in excellent agreement with the other branches. (ii) The small branch at ^{107}Pd can still account for about 10 percent of the abundance of ^{108}Cd. (iii) The value for the branching ratio at ^{204}Tl is in reasonable agreement with that obtained by Blake and Schramm (1975) and Macklin and Winters (1976).

Since we have preferred the exponential $\rho(\tau)$ in our calculations, we can note another appealing feature for its exact solution. Extending the results of CFHZ to include the creation of α-particles by neutron capture on ^{209}Bi, the number of neutron captures per seed nucleus is given by

$$n_c(\tau) = \sum_{A=56}^{209} (A - 56) \frac{\psi_A(\tau)}{\sigma_A} + 4 \int_0^\tau \psi_{209}(\tau') d\tau' . \tag{74}$$

TABLE 2

BRANCHING TIME SCALES AT $T_8 = 3.1$, $n_n = 1.6 \times 10^7$ cm^{-3}*

Branching Nuclide	σ (mb)	t_β(Lab) (yr)	f_β	$t_\beta(T_8)$ (yr)	$t_n(T_8)$ (yr)
^{63}Ni	30	1.0(2)	0.66	100	190
^{64}Cu	...	1.5(−3)	0.64	...	...
^{81}Kr	450	2.1(5)	0.51	12	13
^{99}Tc	800	2.1(5)	0.56	5.6	7.2
^{107}Pd	950	6.5(6)	0.0066	910	6.0
^{129}I	450	1.6(7)	0.96	0.55	13
^{135}Cs	200	2.3(6)	0.29	71	29
^{147}Pm	1100	2.6	0.67	2.6	5.2
^{153}Gd	2500	0.66	0.78	0.63	2.3
^{155}Eu	1700	4.8	>0.41	<4.8	3.4
^{160}Tb	4100	0.20	0.87	0.20	1.4
^{170}Tm	3200	0.35	0.84	0.35	1.8
^{171}Tm	1300	1.9	0.70	1.9	4.4
^{182}Ta	2300	0.32	0.89	0.32	2.5
^{192}Ir	2100	0.20	0.93	0.20	2.7
^{193}Pt	1100	5.0(1)	0.031	160	5.2
^{204}Tl	134†	3.8	0.92	3.8	43
^{205}Pb	54†	1.4(7)	0.45	130	105

NOTE.—$a(b) \equiv a \times 10^b$.

* Calculated at $\rho = 2000$ g cm^{-3}. The temperature and neutron density are chosen as representative mean values from Table 1.

† Taken from Macklin and Winters 1976.

Since $\rho(\tau)d\tau$ is defined as the number of seed nuclei exposed to an integrated flux τ in the interval $d\tau$, the average number of neutron captures *per exposed seed* is then

$$N_c \equiv \int_0^\infty \rho(\tau) n_c(\tau) d\tau \Big/ \int_0^\infty \rho(\tau) d\tau \, .$$

Using equation (74), the single exponential $\rho(\tau) = G \exp(-\tau/\tau_0)$ yields the analytical result

$$N_c(\tau_0) = \sum_{A=56}^{205} \frac{(A-56)}{\tau_0 \sigma_A} P(56, A) + P(56, 205) \left\{ \frac{\sum_{A=206}^{209} [(A-56)/\tau_0 \sigma_A] P(206, A) + 4P(56, 209)}{1 - P(206, 209)} \right\}, \quad (75)$$

with

$$P(r, s) \equiv \prod_{i=r}^{s} \left(1 + \frac{1}{\tau_0 \sigma_i}\right)^{-1},$$

and where we have explicitly included the terminal cycling among the isotopes of Pb and Bi (Clayton and Rassbach 1967); the *total* number of neutron captures required would then be $G\tau_0 N_c(\tau_0)$. Analogous results can be easily generated for any superposition of exponentials. In Figure 15 we have plotted $N_c(\tau_0)$ as given by equation (75) for the unique *s*-process path. It is readily apparent that $N_c(\tau_0 = 0.25) = 4.8$ is required by the large-A region of the solar-system σN curve, with a total of $\sim 8.5 \times 10^3$ neutrons (per 10^6 Si atoms) captured; fitting the $A < 75$ portion with $\tau_0 = 0.1$ demands only 1.5 captures per seed nucleus. We can now go one step further and inquire as to the total exposure time that is required. Again following CFHZ, the instantaneous capture rate of a given distribution is $dn_c/d\tau$, so that a measure of the "mean time," $\langle t \rangle$, required with exposure to a constant neutron flux is

$$\langle t \rangle \equiv \left[\Phi \int_0^\infty \rho(\tau) \frac{dn_c(\tau)}{d\tau} d\tau \Big/ \int_0^\infty \rho(\tau) n_c(\tau) d\tau \right]^{-1} = \frac{\tau_0}{\Phi} \, . \quad (76)$$

This last form [for an exponential $\rho(\tau)$] is preferable to a simple sum of half-lives along the chain, since it weights the contribution of each species correctly with the relative abundance it achieves. Figure 15 also contains a graph of $\langle t \rangle$ (with the neutron flux measured in units of 10^{15} cm^{-2} s^{-1}) as a function of the parameter τ_0. Using our value $\Phi = 3.5 \times 10^{15}$ cm^{-2} s^{-1}, we find specifically that $\langle t \rangle = 2270$ years for $\tau_0 = 0.25$ and $\langle t \rangle = 907$ years with $\tau_0 = 0.10$. Since these mean times are actually lower limits ("e-folding" times), we can say that the solar system's heavy *s*-process elements required at least several thousand years of exposure time to attain the observed distribution.

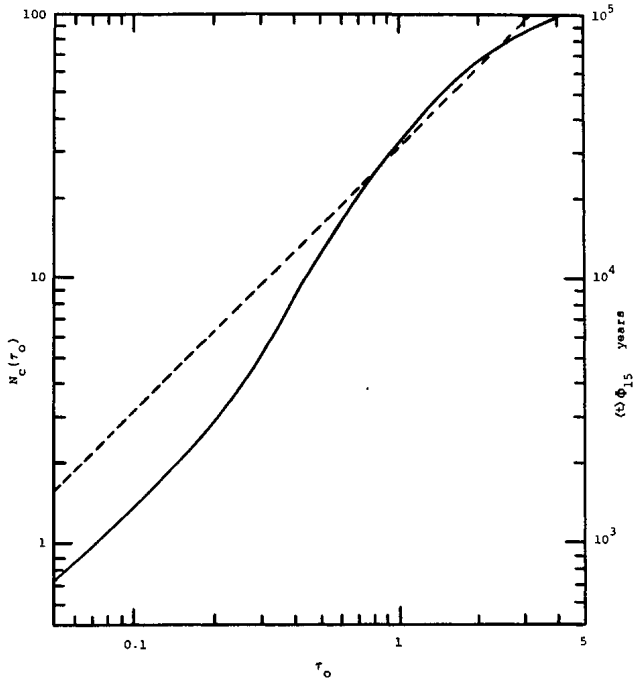

FIG. 15.—The average number of neutron captures per exposed iron seed and the mean time required to generate the *s*-process abundance distribution for an exponential $\rho(\tau)$. The scale for $N_c(\tau_0)$ (*solid curve*) is shown on the left margin while that for $\langle t \rangle \Phi_{15}$ (*dashed curve*) is on the right. Φ_{15} is the neutron flux in units of 10^{15} cm^{-2} s^{-1}

In closing we should note that while many of our numerical results may change with time as more experimental data becomes available, the formal framework and expressions we have developed for considering the effects of *s*-process branching should nevertheless prove to be useful tools.

One of us (R. A. W.) thanks the Fannie and John Hertz Foundation for a predoctoral fellowship. This research was supported by the National Science Foundation grants GP-18335 and MPS 74-20076.

REFERENCES

Allen, B. J., Gibbons, J. H., and Macklin, R. L. 1971, *Adv. Nucl. Phys.*, **4**, 205.
Amiet, J. P., and Zeh, H. D. 1968, *Zs. f. Phys.*, **217**, 485.
Audouze, J., Fowler, W. A., and Schramm, D. N. 1972, *Nature*, **238**, 8.
Audouze, J., and Truran, J. W. 1975, *Ap. J.*, **202**, 204.
Bahcall, J. N. 1964, *Ap. J.*, **139**, 318.
Blake, J. B., and Schramm, D. N. 1973, *Ap. J.*, **179**, 569.
———. 1975, *ibid.*, **197**, 615.
Burbidge, E. M., Burbidge, G. R., Fowler, W. A., and Hoyle, F. 1957, *Rev. Mod. Phys.*, **29**, 547.
Cameron, A. G. W. 1959, *Ap. J.*, **130**, 452.
———. 1973, *Space Sci. Rev.*, **15**, 121.
Clayton, D. D. 1964, *Ap. J.*, **139**, 637.
———. 1965, in *Nucleosynthesis*, ed. W. D. Arnett, C. J. Hansen, J. W. Truran, and A. G. W. Cameron (New York: Gordon and Breach), p. 225.
———. 1968, *Principles of Stellar Evolution and Nucleosynthesis* (New York: McGraw-Hill).
Clayton, D. D., Fowler, W. A., Hull, T. E., and Zimmerman, B. A. 1961, *Ann. Phys.*, **12**, 331 (CFHZ).
Clayton, D. D., and Newman, M. J. 1974, *Ap. J.*, **192**, 501.
Clayton, D. D., and Rassbach, M. E. 1967, *Ap. J.*, **148**, 69.
Clayton, D. D., and Ward, R. A. 1974, *Ap. J.*, **193**, 397.
Gleit, C. E., Tang, C.-W., and Coryell, C. D. 1968, *Nucl. Data Sheets*, **13**, 5-5-109.
Hainebach, K. L., Clayton, D. D., Arnett, W. D., and Woosley, S. E. 1974, *Ap. J.*, **193**, 157.
Holmes, J., and Woosley, S. E. 1976, in preparation.
Iben, I., Jr. 1975, *Ap. J.*, **196**, 525.
Lederer, C. M., Hollander, J. M., and Perlman, I. 1967, *Table of Isotopes* (6th ed.; New York: Wiley).
Macklin, R. L., and Winters, R. R. 1976, in preparation.
Mason, B., ed. 1971, *Handbook of Elemental Abundances in Meteorites* (New York: Gordon and Breach).
Newman, M. J., M.S. thesis, Rice University (unpublished).
Nuclear Data Sheets, ed. Nuclear Data Group, D. J. Horen, Director (New York: Academic Press).
Perrone, F. A., and Clayton, D. D. 1971, *Ap. and Space Sci.*, **11**, 451.
Peterson, V. L., and Tripp, D. A. 1973, *Ap. J.*, **184**, 473.
Reeves, H. 1966, *Ap. J.*, **146**, 447.
Sanders, R. M. 1967, *Ap. J.*, **150**, 971.
Schwarzschild, M., and Härm, R. 1967, *Ap. J.*, **150**, 961.
Seeger, P. A., and Fowler, W. A. 1966, *Ap. J.*, **144**, 822.
Seeger, P. A., Fowler, W. A., and Clayton, D. D. 1965, *Ap. J. Suppl.*, **11**, p. 121.
Shaw, P. B., and Clayton, D. D. 1967, *Phys. Rev.*, **160**, 1193.
Stroud, D. B. 1972, *Ap. J.*, **178**, L93.
Suess, H. E., and Zeh, H. D. 1973, *Ap. and Space Sci.*, **23**, 173.
Truran, J. W., and Kozlovsky, B.-Z. 1969, *Ap. J.*, **158**, 1021.
Ulrich, R. K. 1973, in *Explosive Nucleosynthesis*, ed. D. N. Schramm and W. D. Arnett (Austin: University of Texas Press), p. 139.
Weigert, A. 1966, *Zs. f. Ap.*, **64**, 395.

DONALD D. CLAYTON and RICHARD A. WARD: Department of Space Physics and Astronomy, Rice University, Houston, TX 77001

MICHAEL J. NEWMAN: W. K. Kellogg Radiation Laboratory 106–38, California Institute of Technology, Pasadena, CA 91125